Tensile Microcracking Behavior of Granites After High Temperature Treatment by Considering the Effect of Grain Size and Mineralogical Composition

Tensile Microcracking Behavior of Granites after High Temperature Treatment by Considering the Effect of Grain Size and Mineralogical Composition

Xunjian Hu[1,2,*], Giuseppe Lacidogna[2], Ni Xie[3], Pedro Marin Montanari[2], Xiaonan Gong[1]

[1] Research Center of Coastal and Urban Geotechnical Engineering, Zhejiang University, Hangzhou 310058, China

[2]Department of Structural, Geotechnical and Building Engineering, Politecnico di Torino, Corso Duca Degli Abruzzi 24, 10129 Turin, Italy

[3]Faculty of Engineering, China University of Geosciences (Wuhan), Wuhan 430074, China

* Corresponding author: huxunjian2021@zju.edu.cn

Highlights:

1. Grain size and mineralogical composition of pre-heated granites significantly influence their tensile microcracking behavior and mode I fracture toughness;
2. In contrast to fine-grained granites, coarse-grained granites exhibit a pronounced brittle-ductile transition in the temperature range of 400 °C to 600 °C;
3. The tortuosity of fracture paths varies with grain size and temperature, with notable variations observed in both coarse- and medium-grained samples after high temperature treatment.

Abstract:

The tensile microcracking behavior of granites, significantly influenced by temperature, is crucial in high temperature geological and engineering applications such as geothermal energy system and nuclear waste disposal. This study investigates the impact of grain size and mineralogical composition on the mechanical properties and microcracking behavior of pre-heated granites and underlying mechanisms through a comprehensive comparative analysis. Utilizing three-point semi-circular bending tests, three distinct granite types differing in grain size and mineralogical composition were subjected to varying temperature treatments ranging from 25 °C to 1000 °C. Detailed thin-section analyses were conducted to examine the morphologies of post-failure specimens, elucidating the underlying mechanisms governing microcracking behavior. Results indicate that granites with larger average grain sizes and heterogeneous grain size distributions exhibit heightened sensitivity to thermal treatment, manifesting in increased thermal crack density. Fracture surface topographies vary with mineralogical composition and treatment temperature, with distinct patterns such as conchoidal fracture and lamellar tearing crack observed at different temperature ranges. Grain size and mineral composition significantly influence load-displacement curves and mode I fracture toughness, with a notable brittle-ductile transition observed in coarse-grained granites between 400 °C and 600 °C. Fracture toughness decreases with increasing temperature and grain size. Furthermore, grain size impacts the tortuosity of fracture paths under mode I loading, particularly pronounced in coarse- and medium-grained granites. In medium-grained granites, the tortuosity and width of fracture paths increase with treatment temperature, whereas the effect of temperature on the tortuosity of fracture paths in fine-grained granites is negligible.

Keywords: Granite; Semi-circular bending test; High temperature; Tensile microcracking behavior; Grain size; Mineralogical composition.

1. Introduction

The comprehension of tensile cracking behavior in rocks holds paramount importance for various engineering applications, including the construction of rock slopes (Gao et al. 2017), tunnel excavation projects (Zhu et al. 2022), and the production of geothermal energy (Feng et al. 2020). Particularly in Enhanced Geothermal Systems (EGS), hydraulic fracturing to generate fracture networks is a critical process for augmenting the productivity of geothermal reservoirs (Olasolo et al. 2016). This necessitates a thorough investigation into the initiation and propagation mechanisms of fractures induced by hydraulic fracturing to improve energy recovery. Additionally, granite, as a quintessential crystalline rock, plays a pivotal role in numerous scientific and engineering domains. It is predominantly present in hot dry rock reservoirs (Breede et al. 2013) and serves as the host rock in nuclear waste disposal systems (Zuo et al. 2017). Temperature within hot dry rock reservoirs ranges from 150 °C to 500 °C at depths of 5~6 km (Gallup 2009), while temperatures in nuclear waste disposal sites may exceed these values owing to the heat released during the decay process of high-level radioactive waste (Gibb 2000; Zuo et al. 2017). The cracking behavior of rock is intricately linked to its thermal environment (Zuo et al. 2017; Hu et al. 2023a). Consequently, an in-depth understanding of cracking behavior of granites under elevated temperatures is instrumental in assessing the safety and enhancing the efficiency of rock engineering projects.

Fracture mechanics identify three primary modes of fracturing: (a) mode I (opening mode), characterized by purely tensile stresses acting perpendicular to the crack propagation direction without any relative slip between the crack faces; (b) mode II (in-plane shear mode), where the stress field around the crack plane exhibits antisymmetric; and (c) mode III, encompasses both tensile and shear stresses. Considering the inherently low tensile strength of rock materials, exploring the crack propagation in rocks under mode I loading conditions constitutes a fundamental issue (Zhang 2002). A number of experimental studies have investigated the cracking behavior of granite under mode I loading (Yu et al. 2018; Wong et al. 2019; Guo and Wong 2020; Alneasan and Behnia 2021; Braunagel and Griffith 2022; Guo and Zhao 2022; Alneasan and Alzo'ubi 2023), focusing on the variations in macroscopic mechanical properties and cracking behavior, including fracture toughness, crack tip velocity, and the evolution of fracture process zone.

Granite is inherently heterogeneous, comprising various mineral grains and microstructures that

significantly influence its response to mechanical loading. The micro-mechanisms dictating the cracking behavior of granite under load have been categorized into three different groups (Mo et al. 2023): (a) mineral grain effect (e.g., grain shape and grain size); (b) microstructural effect (e.g., cleavage and grain boundary); and (c) combinations of (a) and (b). These factors govern the mechanical properties of fractures, such as toughness and failure mode (brittle or ductile), as well as fracture morphology, including fracture path and roughness. Previous studies indicate that the mineral heterogeneity caused local tensile stress concentration and thereby influencing the cracking behavior and mechanical properties of rocks (Lan et al. 2010). Specifically, mineral cleavage significantly impacts the fracture path and its roughness (Mo et al. 2023). Parameters such as rupture speed, fracture toughness and fracture path tortuosity of granite under mode I loading are closely related to its grain size and mineralogical composition (Sabri et al. 2016; Alneasan and Behnia 2021; Aghababaei et al. 2024). Investigations into the impact of grain size on the fracture toughness and tensile strength of granite reveals a general decrease in fracture toughness with increasing grain size (Yu et al. 2018). However, other findings suggest that granite with a medium grain size of 3 mm exhibits optimal fracture toughness (Sabri et al. 2016). This apparent contradiction highlights that fracture toughness may increase with larger grain sizes (Aghababaei et al. 2024). These variations underscore the complexity of the role played by other microstructural features, such as mineralogical composition and grain shape (Alneasan and Behnia 2021).

Granite typically comprises minerals such as quartz, K-feldspar, plagioclase, and biotite. Nanoindentation tests reveal that quartz has the highest average fracture toughness (5.34 $MPa \cdot m^{1/2}$), followed by K-feldspar (4.83 $MPa \cdot m^{1/2}$), plagioclase (2.70 $MPa \cdot m^{1/2}$), and biotite (2.41 $MPa \cdot m^{1/2}$) (Liu et al. 2023). Consequently, granite with a higher quartz content is expected to exhibit greater fracture toughness compared to granite predominantly composed of plagioclase. Numerous studies have qualitatively and quantitatively indicated that mineral grain and microstructural effects significantly influence the mechanical behavior of granite (Hu et al. 2020, 2023b; Alneasan and Behnia 2021; Mo et al. 2023). However, the relationship between the cracking behavior and microstructural characteristics of granite remains inadequately understood despite some progress.

Significant advancements have been made in understanding the cracking processes and fundamental mechanisms in granite at room temperature. However, high temperatures introduce additional complexity to these phenomena. For example, mineral grain size critically affects the

uniaxial and triaxial compressive strengths (Shao et al. 2014; Kang et al. 2021; Wong et al. 2023; Yin et al. 2021) and Brazilian tensile strength (Zhao et al. 2018) of rocks after high temperature treatment. Similarly, mineral grain and microstructural effects significantly impact the fracture toughness of rocks after high temperature treatment (Mahanta et al. 2016; Peng et al. 2020; Alneasan et al. 2022). This phenomenon is closely related to the mineral composition of granite and the differential thermal expansion of its mineral grains. The different thermal expansion coefficients among mineral grains lead to a heterogeneous distribution of thermal stresses (Feng et al. 2021; Hu et al. 2023b), which changes the microstructure and thus the macroscopic mechanical properties of granite. This suggests that the thermomechanical behavior of granite is intricately linked to its mineralogical characteristics, including grain size, shape, and composition.

At high temperature, rock may experience a series of microstructural changes, such as crystal expansion (Wong and Brace 1979), microcrack generation and propagation (Kranz 1983), hot melting (Heuze 1983), and phase transformation (Glover et al. 1995). Consequently, the microstructural characteristics of granite (e.g., mineral composition and grain size) directly affect the degree of thermal cracking and further affect the cracking behavior and mechanical properties of granite at high temperature. Under mode I loading, the fracture path is influenced by grain size and mineralogy; smaller grain sizes reduce fracture path width and tortuosity, resulting in straighter fracture paths (Alneasan and Behnia 2021). The mineral clustering and mineral composition also play a critical role in the fracture path of rocks under mode I loading (Zhang et al. 2019; Guo and Zhao 2022). Therefore, a comprehensive analysis of grain-scale fracture paths in granite with diverse textural characteristics at elevated temperatures is essential.

However, most existing studies focus on the analysis of grain-scale fracture paths in rocks at room temperature under mode I loading (Alneasan and Behnia 2021; Guo and Zhao 2022; Braunagel and Griffith 2022; Aghababaei et al. 2024), or limit their scope to a single rock type with same grain size and mineral composition (Kataoka et al. 2015; Zhang et al. 2019). Furthermore, the characteristics of thermally induced microcracks (e.g., density and orientation) of different granite types have been seldom explored. To address this research gap, a comprehensive experimental investigation was conducted to study the tensile microcracking behavior of three types of semi-circular bending (SCB) granite samples after different temperature treatments (including 25 °C, 200 °C, 400 °C, 600 °C, 800 °C, and 1000 °C, respectively). The effect of grain size and mineralogical

composition on fracture toughness, fracture path, tortuosity and fracture width of granite after high temperature treatment were investigated. To elucidate the reasons for the variations in mechanical properties observed across three granite types from a microscopic standpoint, microscopic analyses were performed on thin-section samples.

2. Materials and Methods

Granite, an igneous rock resulting from magma condensation, is extensively found in the upper crust of earth. Its significant strength and minimal permeability (Wang et al. 2018) make it an important reservoir material for geothermal system, which reach temperatures up to 650 °C (Wu et al. 2019), and an important rock type for nuclear self-storage, which reach temperatures up to 1300 °C (Gibb 2000; Ranjith et al. 2012; Shao et al. 2014). The notable strength of granite is crucial in defining its brittle behavior, thereby making it a subject of interest for various studies investigating the temperature-dependent cracking processes.

2.1. Mineralogical composition

The samples used in this work were collected from Shandong Peninsula in China (Fig. 1a). The Shandong Peninsula, located in the eastern North China Craton, is divided by the central Tan-Lu Fault Zone into Luxi and Jiaodong terranes (Yang et al. 2021). Two representative types of rocks were sampled from the Luxi terrane, and one type of rock was sampled from the Jiaodong terrane near Wulian-Yantai Fault (Fig. 1b). Thin sections (Fig. 2) were prepared to analyze the grain size, through image analysis such as grain boundary maps using ImageJ software (https://imagej.net/). By grain size grading, the granite samples were divided into three types: coarse-grained (CG) granite (Fig. 2a), medium-grained (MG) granite (Fig. 2b), and fine-grained (FG) granite (Fig. 2c).

The mineral content of the samples was determined using the X-ray diffractometer (Table 1). The three rock types exhibit nearly identical mineralogical compositions but differ significantly in terms of mineral percentages and grain sizes. As shown in Table 1, Feldspar (including microcline and albite) is a fundamental component in all three rock types and is anticipated to significantly influence their cracking and mechanical behaviors. The quartz content varies notably among the three granites, with CG samples (20.1%) and MG samples (9.6%) having substantially higher quartz percentages than FG samples (3.9%). Therefore, quartz emerges as a critical mineral in CG samples and MG samples.

Despite the quartz content disqualifying MG samples and FG samples from being classified as granite according to the International Union of Geological Sciences (IUGS) criteria (Le Maitre et al. 2005), the similarity in mineral compositions and the complexities of geological nomenclature warrant their designation as granite in this investigation.

Fig. 1 Schematic geological maps of the study areas with sample localities. **a** geographical position of the study area in China; **b** geological sketch map of Shandong Peninsula (after Yang et al. 2021). Note: green points in (**b**) show location of three studied granites.

Fig. 2 Thin section of three types granites. **a** coarse-grained granite (CG); **b** medium-grained granite (MG); **c** fine-grained granite (FG). Qtz: quartz, Mcc: microcline, Hbl: hornblende, Bt: biotite, Ab: albite.

Table 1 Mineralogical composition of the three rock types at room temperature

2.2. Grain size distribution

Grain size is a crucial important microscopic characteristic of rocks, affecting the short-term and long-term strength (Peng et al. 2017; Atapour and Mortazavi 2018; Hu et al. 2023c), hydraulic fracturing properties (Huang et al. 2019), and associated microcrack behavior of rocks. In general, each of rock samples has a unique grain size distribution. Based on the digital microscopic images of thin sections (e.g., Fig. 2), the grain size distributions of the three types of granites were analyzed and are presented in Fig. 3. The average grain sizes of the CG, MG, and FG granite samples were approximately 3.67, 1.74, and 0.18 mm, respectively. The grain size distributions generally follow the lognormal distribution (red curves in Figs. 3a~3c), which is similar to Hong Kong granite (Guo and Wong 2020).

Figure 3d highlights the heterogeneity in grain size distribution, revealing that the CG samples exhibit a more heterogeneous distribution, while FG samples display a more homogeneous distribution. Presently, several metrics exist for the quantitative assessment of grain size heterogeneity. However, due to the complexity of this characteristic, these metrics often do not capture its full extent (Peng et al. 2017; Kang et al. 2021; Hu et al. 2023b). Therefore, this study adopts a qualitative rather

than a quantitative description of grain size heterogeneity.

Fig. 3 Grain size distribution of three granite samples. **a** CG; **b** MG; **c** FG; **d** cumulative grain size distributions of samples. The red curves in (**a**), (**b**) and (**c**) represent the log-normal fitting curves of the grain size distribution. SD: standard deviation.

2.3. Specimen preparation

The SCB specimen (Fig. 4a) is widely used to assess mode I fracture toughness of brittle materials due to its straightforward specimen preparation process (Kuruppu and Chong 2012; Kuruppu et al. 2014). The SCB specimen geometry used in this study aligns with the specifications detailed by Guo and Wong (2020). To prepare the specimen, a rock core with a radius of 42 mm and a thickness of 33.6 mm was bisected along its diameter to create two semi-discs. A straight notch, measuring 21 mm in length and 0.7 mm in width, was then introduced perpendicular to the cut, originating from the center of the disc. The SCB specimens of CG, MG, and FG granite specimens are shown in Figs. 4b, 4c, and 4d, respectively.

The specimens were subjected to thermal treatment in a muffle furnace capable of reaching a maximum temperature of 1200 °C, as illustrated in Fig. 4e. They were progressively heated to predetermined temperatures (200 °C, 400 °C, 600 °C, 800 °C, and 1000 °C, respectively) at a controlled rate of 5 °C per minute. Each target temperature was maintained for 4 hours to ensure thorough heating. After heating, the specimens were allowed to cool at the same controlled rate.

Fig. 4 Experimental study. **a** geometry of semi-circular bend specimen; **b** CG specimen; **c** MG specimen; **d** FG specimen; **e** muffle furnace; **f** Leica DM750P polarization microscopy; **g** LJ-16 ion sputtering instrument; **h** Thermo Scientific Scios 2 scanning electron microscopy; **i** universal testing machine; **j** detailed position of SCB specimen.

2.4. Microscopic examination

The Leica DM750P polarization microscopy (Fig. 4f) was used to study the microcrack distribution of specimens after high temperature treatment. For the purpose of polarization analysis, the specimens were prepared as coin-shaped discs, each 10 mm in diameter and 0.5 mm thick, and

underwent the identical thermal procedures as the SCB specimens across various temperatures. Similar to the polarizing microscopy technique, the scanning electron microscope (SEM) has been widely used in laboratory tests to assess thermal damage in rocks. To enhance its electrical conductivity for SEM observation, the specimen surfaces were coated with gold powder using an ion sputtering device (Fig. 4g). The Thermo Scientific Scios 2 (Fig. 4h) was then utilized to examine the fracture surfaces of specimens subjected to high temperature treatments. The specimens prepared for SEM analysis were coin-shaped, with a diameter of 2.5 mm and a height of 0.5 mm, and treated by exactly the same procedures as that of the SCB and thin-section specimens in different temperatures.

To elucidate the differences in mechanical properties among the three types of granites at a microscopic level, microscopic observations were performed on thin-section samples containing macrocracks from the failed SCB specimens using polarization microscopy (Fig. 4f). The preparation of these thin-section samples followed the method described by Guo and Zhao (2022). Initially, the failed specimens (Fig. 5a) were glued with epoxy at room temperature for 48 hours. A cuboidal segment, encapsulating the macrocrack and measuring approximately 25 mm in length, 2.5 mm in width, and 5 mm in thickness, was then excised from the core of the failed specimen (Fig. 5b). The region of interest in this work was the narrow area containing the macrocrack (Fig. 5c). Subsequently, standard thin-section samples with 0.03 mm thickness were prepared from the cuboid samples (Fig. 5d). These thin-section samples containing macrocrack were examined using Leica DM750P polarization microscopy (Fig. 4f).

Fig. 5 Preparation procedures of the thin-section samples containing the macroscopic fracture. **a** failed sample under mode I loading; **b** position of thin-section sample; **c** region of interest; **d** thin-section sample for polarizing microscopy observation.

2.5. Semi-circular bending (SCB) test

This study focuses on investigating the impact of high temperature treatment and rock microstructure on fracture toughness and cracking behavior under mode I loading. The SCB specimens were subjected to static loading, where specimens underwent symmetric three-point bending with a span distance of 50 mm (Fig. 4a) until failure occurred. The mode I fracture toughness (K_{IC}) of the samples was subsequently determined based on the peak load (P_{max}) and the geometric

parameters of the SCB specimens, as outlined by Kuruppu et al. (2014):

$$K_{IC} = Y' \frac{P_{\max} \sqrt{\pi a}}{2RB} \tag{1}$$

$$Y' = -1.297 + 9.516(S/R) - \left(0.47 + 16.457(S/R)\right)\beta + \left(1.071 + 34.401(S/R)\right)\beta^2 \tag{2}$$

where a is the length of notch, R is the radius of samples, B is the thickness of samples, S is the half span distance, $\beta=a/R$, and Y' is the critical stress intensity factor.

In this work, the SCB tests were carried out using a universal testing machine (Fig. 4i) in the displacement control mode at the rate of 0.02 mm/min. The loading system comprises a loading and measurement device connected to a PC, with the SCB sample positioned on two support rollers (Fig. 4j). Testing concluded upon detection of a notable decrease in axial force, indicating failure of the SCB specimens.

3. Results

3.1. Macroscopic and microscopic characteristics after high temperature treatment

3.1.1. Macroscopic surface characteristics

Figure 6 shows the SCB samples after high temperature treatment (including 25 °C, 200 °C, 400 °C, 600 °C, 800 °C, and 1000 °C). The surface color and appearance of three types of samples change progressively with increasing temperature. For example, the surface colors of the CG samples (Fig. 6a) transitions from black-gray to reddish-gray up to 400 °C, turning white-gray beyond 600 °C. Similar changes in surface color are observed in the MG (Fig. 6b) and FG (Fig. 6c) samples, albeit with slight variations. In these samples, the color shifts from black-gray to reddish-brown, notably accentuated after exposure to 1000 °C. These variations in color among granite types are partly attributable to their respective mineralogical compositions (see Table 1). A consistent observation across all samples is the alteration of dark minerals like biotite and hornblende, changing from black to golden-brown, a phenomenon supported by earlier studies (Vazquez et al. 2021).

A notable observation is the development of visible macro-scale thermal cracks (indicated by red lines in Fig. 6a) in CG granite specimens exposed to elevated temperatures of 600 °C, 800 °C, and 1000 °C. With increasing temperature, both the frequency and size of these thermal cracks become

more pronounced. Notably, at 1000 °C, the CG specimen experienced macro-scale structural failure (highlighted by a blue box in Fig. 6a), resulting in complete loss of load-bearing capacity. However, such damage was not observed on the surfaces of all MG (Fig. 6b) and FG (Fig. 6c) samples.

Despite their mineralogical similarities, this discrepancy suggests that granites with larger average grain sizes and more heterogeneous grain size distributions (as shown in Fig. 3) are more susceptible to thermal treatments. Differences in mineral types during heating induce thermal stress imbalances due to differential thermal expansion. Larger variations in grain size among neighboring mineral grains result in significantly higher unbalanced tensile thermal stresses, facilitating the initiation of microcracks more readily. This phenomenon is supported by experimental findings (Shao et al. 2014; Kumari et al. 2019; Kang et al. 2021) and theoretical models (Feng et al. 2021). Consequently, CG granite specimens, characterized by larger average grain sizes and more heterogeneous grain size distributions, are more prone to developing visible macro-scale thermal cracks. These thermal cracks in CG granite specimens lead to a substantially higher volumetric expansion compared to FG and MG granite specimens. Furthermore, the occurrence of visible macro-scale thermal cracks in CG granite specimens results in the generation of significant powder and clasts from the surface (Fig. 6a), phenomena rarely observed in FG and MG granite specimens (Figs. 6b and 6c). Additionally, high temperature treatment induces the release of structural or bonded water, as well as the recrystallization and decomposition of minerals (Wong et al. 2020), contributing to variations in rock mass following high temperature exposure (Sun et al. 2017; Wong et al. 2020). These factors make the mass of CG granite specimens more variable compared to FG and MG granite specimens (Kang et al. 2021).

Fig. 6 Appearance of three types of granite specimens after high temperature treatment. **a** CG specimens; **b** MG specimens; **c** FG specimens.

3.1.2. Microscopic crack characteristics

Optical microscopy analysis revealed the microstructural heterogeneity of three rock types, as shown in Fig. 2. Grain boundaries in CG and MG specimens are clearly visible in optical images, whereas those in FG specimens are less distinct due to their smaller grain sizes (Fig. 3). After high-temperature treatment, rock materials exhibiting significant heterogeneity developed numerous

thermally induced microcracks, consistent with findings from previous laboratory tests (Nasseri et al. 2007; Griffiths et al. 2017; Yang et al. 2017; Feng et al. 2020; Zhou et al. 2020; Chen et al. 2022). Notably, changes in rock physical and mechanical properties are associated with these thermally induced microcracks. Detailed examination of post-treatment microstructures aids in understanding the microscale mechanisms responsible for thermal damage in rocks. However, previous studies have primarily focused on the same type of rocks and ignored the effects of mineralogical composition and grain size (Griffiths et al. 2017; Sha et al. 2020; Chen et al. 2022). This study employs optical microscopy under plane-polarized light to examine three distinct rock types after exposure to high temperatures. The investigation focuses on two categories of microcracks at grain-scale identified by Guéguen and Boutéca (2004): (a) grain boundary (GB) cracks, which propagate along grain boundaries, and (b) intra-grain (IG) cracks, which traverse through mineral grains themselves.

To characterize the thermal microcracks qualitatively and quantitatively in the three types of granite studied, microscopic analysis was conducted on thin-sections prepared from the thermally treated granite samples using an optical microscope. Fig. 7 shows representative thin-section images of the three types of granite after high temperature treatment, revealing notable changes in mineral grains and associated microcracking behavior due to thermal processes. Variations in mineralogical composition and grain size distribution contribute significantly to differing microcracking behavior. Generally, an increase in thermal microcracks is observed as the treated temperature increases gradually from room temperature to 1000 °C. Untreated specimens (25 °C) exhibit minimal pre-existing microcracks, with mineral grains appearing tightly bonded and maintaining relatively intact mineral morphology (Figs. 7a, 7g, and 7m). For example, quartz (Qtz) and microcline (Mcc) in Figs. 7a and 7g exhibit complete structures with minimal internal microcracks. Maintaining complete mineral morphology and well-defined boundaries between minerals are critical for enhancing rock mechanical properties. However, thermal stress induced by high temperature causes irreversible damage to the rock microstructure. At 200 °C (e.g., Fig. 7b) and 400 °C (e.g., Fig. 7c), there is a progressive increase in microcrack density, with heat expansion induced microcracks causing mineral separation, either along mineral boundaries (Fig. 7h) or within the minerals themselves (Fig. 7b). This phenomenon is considered a significant factor contributing to increased permeability in granite (Feng et al. 2021).

Upon further heating to 600 °C (e.g., Fig. 7d) and 800 °C (e.g., Fig. 7e), a profusion of

microcracks becomes apparent, significantly changing mineral morphology, which becomes almost segmented by a complex network of thermally induced cracks. Another noteworthy observation is the pronounced widening of these microcracks, which is consistent with previous experimental results (Homand-Etienne and Houpert 1989; Nasseri et al. 2007; Chen et al. 2022). Numerous thermal microcracks are observed in the specimens heated to 1000 °C (e.g., Fig. 7f), fostering crack interaction and coalescence. This results in a notable increase in crack density and aperture width compared to those observed at 800 °C. Consequently, mineral morphology undergoes substantial disruption, fracturing into numerous smaller segments.

The formation of thermally induced microcracks due to temperature variation is predominantly attributed to the thermal expansion of minerals, as demonstrated in previous studies (Wong et al. 2020; Zhou et al. 2020). Variations in thermal expansion coefficients among different minerals lead to the disruption of original bonds between mineral grains, resulting in the initiation of GB cracks. For example, the thermal expansion coefficient of α-quartz is 24.3×10^{-6} 1/K, which is 8.1 times greater than biotite (3.0×10^{-6} 1/K) (Fei 2005). These discrepancies in thermal expansion coefficients at the same temperature cause volume changes in the minerals, creating mismatches and ultimately inducing GB cracks (Fig. 7i). Furthermore, substantial disparities in thermal expansion coefficients are observed not only among different types of minerals (Fei 2005) but also within a single mineral species. For example, biotite exhibits different thermal expansion coefficients along the *a*-, *b*-, and *c*-axis (Chon et al. 2003; Fei 2005; Zhou et al. 2020), potentially leading to the development of IG cracks. In addition to thermal expansion, variations in the strength and deformation characteristics within the same mineral (Lamberson and Ramesh 2015; Hu et al. 2020) affect the capacity of minerals to endure thermal stress across different locations. This results in the irregular initiation and growth of cracks, propagating along the paths requiring the least energy, as confirmed by optical images (Fig. 7).

Fig. 7 The representative thin-section images of the three types of granites after high temperature treatment. Red arrows indicate grain-boundary (GB) cracks and pure blue arrows indicate intra-grain (IG) cracks. Qtz: quartz, Mcc: microcline, Hbl: hornblende, Bt: biotite, Ab: albite.

Variations among different granite types arise from microstructural features that influence the formation of thermally induced cracks. CG samples have larger average grain sizes and more

heterogeneous grain size distributions, leading to greater thermal stress from temperature changes (Feng et al. 2021). Consequently, CG samples subjected to high temperature treatments exhibit a more extensive network of thermally induced cracks and greater fragmentation of mineral blocks (Figs. 7b~7f). This correlates with the increased presence of visible macro-scale thermal cracks on CG sample surfaces (Fig. 6). Conversely, the more homogenous grain size distribution in FG samples results in a more even distribution of thermal stress, thereby reducing the propensity for thermal crack formation. Additionally, mineralogical composition influences the crack development inside rocks. For example, quartz volume expansion is about four times higher than that of feldspars (Siegesmund et al. 2008), suggesting that quartz-rich rocks may achieve a denser structure and higher strength through thermal expansion (Wong et al. 2020). However, the three rock types studied in this work are feldspar-rich. The anisotropy of thermal expansion appears to be intrinsic to the tetrahedral framework topology of all feldspars (Tribaudino et al. 2010). Despite this, the complex interplay between mineralogical composition and thermal expansion complicates the precise delineation of this relationship. It was determined that in the three types of rocks studied, grain size has a greater impact on the thermal microcracking behavior (e.g., crack density and propagation path) than mineralogical composition.

To quantitatively characterize the thermal microcracks, their density and orientation were determined using optical images analyzed with ImageJ software. Linear crack density is defined as the ratio of the total length of microcracks to the area of the examined region. It has been widely used to geometrically characterize the crack density and associated microcrack damage inside the rock specimens (Rong et al. 2018; Hu et al. 2023b). For each temperature, five representative optical images were taken at the same scale factor, and statistics of crack density and orientation were generated. In this work, the linear crack density is the average density of five optical images, while the orientation statistics are the aggregate. Each examined region (the area of optical image) is 6.93 mm^2 as shown in Fig. 7. Table 2 and Fig. 8 show the statistical results for the linear crack density of three types of rocks and the orientation distribution of microcracks in CG samples. The orientation of microcrack is defined by the angle between the horizontal direction and microcrack direction in a clockwise direction (0°~180°) and taking 10° as the angle interval.

Table 2 The linear thermal crack density of three types of rocks after treatment at different temperatures

Fig. 8 The orientation distribution of thermally induced cracks within CG samples.

The results for three types of rocks CG, MG, and FG show that as the applied temperature increases from 25 °C to 1000 °C, the linear crack density increases continuously (Table 2). Specifically, the linear crack density in the CG sample rises from 0.37 mm/mm² at 25 °C to 4.34 mm/mm² at 1000 °C, marking an approximate increase by a factor of 11.73 compared to the initial state. These findings are consistent with previous experiments (Nasseri et al. 2007; Griffiths et al. 2017). However, as the average grain size decreases and the mineralogical composition changes, this ratio decreases to 9.52 in MG samples and 6.02 in FG samples. These results underscore the significant impact of grain size and mineralogical composition on crack density variation in granite. In summary, granites with larger average grain sizes and more heterogeneous grain size distributions exhibit heightened sensitivity to thermal treatments. Consequently, under identical thermal conditions, FG samples exhibit a reduced density of thermally induced cracks.

Since the orientation distribution statistics of thermally induced cracks within the three types of rocks are similar, Fig. 8 shows the experimental results for CG samples. At lower temperature (e.g., 25 °C~400 °C), microcracks exhibit preferred orientations, mainly concentrated at 0°~30° and 130°~150° at room temperature. However, as the temperature increases, the number of thermally induced microcracks gradually increases (Table 2), reducing the prevalence of these preferred orientations. Microcracks tend to exhibit a uniform distribution under elevated thermal loading, typically ranging from 600 °C to 1000 °C, aligning well with findings from earlier studies (Feng et al. 2020; Chen et al. 2022; Hu et al. 2023b).

In summary, the development of visible thermal macro-scale cracks and microcracks correlates with alterations in the internal microstructure of rocks, influenced by both grain size and mineralogical composition. It is important to note that the analyses of microcracks and macrocracks do not pertain to identical samples or microscopic locations within the same granite sample. Consequently, the selection of the study area may impact the observed data to some extent (Table 2 and Fig. 8). Despite these considerations, the macroscopic and microscopic analyses conducted in this study offer valuable insights into the influence of grain size and mineralogical composition on the microstructural changes in rocks subjected to high temperature treatments.

3.1.3. Fracture surface topography after high temperature treatment

To examine the changes in microstructure attributed to high-temperature exposure, SEM analysis was conducted on three types of granite samples subjected to heat treatment across a range of temperatures from 25 °C to 1000 °C. Fig. 9 shows the representative fracture surface topography of the three types of granites and the variations in topographic micrographs with mineralogical composition and temperature. The fracture surface topography of quartz is primarily characterized by step pattern (Fig. 9a) and river line pattern (Fig. 9b), both resulting from the shear failure of mineral grains (Ma et al. 2020). This is attributed to material separation along a series of crystal planes of varying heights rather than a singular plane, leading to stepped fractures (Yang et al. 2022). Additionally, typical conchoidal fracture in quartz were also observed corresponded to cleavage shear fracturing (Fig. 9c). Factors related to the mineral cleavage fracturing include bond density, elastic modulus, free surface energy, and fracture toughness of the crystallographic planes in dependence on grain size and crystallographic orientation (Armstrong 2015; Brückner et al. 2024). This study showcases one type of surface topographies of cleavage fracturing induced by thermal stress.

As the temperature increases, more diverse fracture surface topographies appear. At 400 °C, the fracture surface topography was still dominated by brittle fractures such as cleavage step (Fig. 9d), with a small number of dimple (Fig. 9e). Dimple pattern formed by the micropore aggregation fracture was observed in the MG sample after high temperature treatment at 400 °C (Fig. 9d). This phenomenon was also confirmed in previous experiments (Zhou et al. 2020; Gao et al. 2023). Stress concentrators around the tips of micro-cavities, such as dimple patterns, become a primary mechanism dominating the cracking behavior of thermal treated granite (Zhou et al. 2020). At 600 °C, there is a notable increase in the quantity of thermally induced cracks, accompanied by the formation of numerous crack branches (Fig. 9f). This shows that the volumetric damaged zone progressively increases with thermal damage, due to higher networking between the damaged grain boundaries and the IG cracks (Nasseri et al. 2007). Higher temperature promotes more heterogeneous thermal stress distribution within the samples, resulting in more potential propagation paths for thermal induced cracks. These complex stress distributions induce stress concentrations near the tips of microcracks, leading to nearly vertical crack branching (Fig. 9f).

At 800 °C, the number of single minerals formed by the disintegration and segregation of complete minerals due to thermally induced cracks increases significantly. Lamellar tearing fractures occur due to the tearing of feldspar (microcline and albite) or biotite which had the lamellar structure (Fig. 9g). Feldspar and mica minerals in granite are rich in cleavage planes. Under high temperature, heterogeneously distributed thermal stress causes extensive crack development between layers. Lamellar tearing fracture is typical phenomenon caused by tensile failure aggregation (Li et al. 2022). The tensile failure also included IG cracks (Fig. 9h) and scaly fracture (Fig. 9i), represented by generally smooth cleavage cracks (Mo et al. 2023). At 1000 °C, thermal induced cracks further propagation and coalescence, eventually forming larger crack networks (Fig. 9j). These networks are generally composed by GB cracks and IG cracks. For example, Fig. 9k shows two IG cracks connected by a GB crack. Due to the massive initiation of random microcracks, such connection can easily occur in those samples subjected to 1000 °C. Additionally, there is a clear sign of melting on the mineral grain surface, contributing to the thermal damage of samples (Fig. 9l). This was also observed in microphotographs from previous studies on high temperature treated granite (Sun et al. 2019).

In summary, the above analysis indicates that grain size exerts minimal influence on the fracture surface topography. This may be attributed to the relatively small scale (~50 μm) of the examined fracture surface topography, which is smaller than the minimum average grain size observed across the three types of samples (0.18 mm). Consequently, the impact of grain size on fracture surface morphology is considered negligible in this context. However, due to the mineral complexity of rocks, the fracture surface topography of mineral grains at different temperatures may appear random and only of qualitative significance. It is evident that temperature and mineralogical composition have a greater influence than grain size on the fracture surface topography. For example, at lower temperatures (e.g., 25~200 °C), brittle shear fracture is prone to occur within quartz (e.g., Fig. 9c). Conversely, at higher temperatures (e.g., 800~1000 °C), tensile fracture seems more likely to occur within feldspars (e.g., Fig. 9g). The rocks examined in this work are classified as feldspar-rich (Table 1). However, the quartz content in the CG samples is still as high as 20.1%. Thus, the substantial presence of hard and brittle quartz in CG samples may facilitate the initiation of thermally induced microcracks following high temperature treatment, potentially enabling the earlier development of visible macro-scale thermal cracks compared to the other two rock types (Fig. 6).

Fig. 9 Scanning electron microscope micrographs of fracture surface topography of granites under different temperatures. **a** step pattern; **b** river line pattern; **c** conchoidal fracture of quartz; **d** cleavage step; **e** dimple pattern; **f** crack branching; **g** lamellar tearing crack; **h** IG crack parallel to cleavage plane; **i** scaly fracture; **j** crack network; **k** two IG cracks connected by a GB crack; **l** mineral melting after 1000 °C treatment. Note: The areas shown were chosen independently of the evolution of the fracture process, and do not necessarily correspond to a specific failure pattern.

3.2. Mechanical behavior

Figure 10 presents the load-displacement curves and corresponding mechanical properties of three types of granite samples varying in grain size and mineralogical composition at different temperatures (25 °C~1000 °C). The behavior of load-displacement curves is significantly influenced by the temperature of samples treatment. At lower temperatures (e.g., 25 °C to 400 °C), the curves exhibit a distinct brittle failure characterized by a sudden drop in load post-peak, indicative of rock burst phenomena observed audibly during SCB tests. Conversely, as temperatures rise into the range of 600 °C to 1000 °C, a transition to ductile failure becomes prominent. This brittle-ductile transition in the granite agrees well with previous works (Chen et al. 2012; Xu et al. 2018; Kang et al. 2021). After undergoing high temperature treatment at 1000 °C (Fig. 6a), the CG sample experienced failure, thereby precluding subsequent SCB testing and resulting in the unavailability of its load-displacement curve. Significant variations are observed in the load-displacement curves of granite samples treated at high temperatures. Post high temperature treatment, the curves of the CG sample exhibit the most pronounced changes, making it challenging to distinguish between the pre-peak elastic phase and the post-peak stage in curves at higher temperatures (e.g., 600 °C and 800 °C shown in Fig. 10a). In contrast, the FG sample treated at 1000 °C still displayed brittle characteristics in its curve (Fig. 10c). These findings underscore the substantial influence of both grain size and mineralogical composition on the load-displacement behavior of granite under mode I loading following exposure to high temperatures.

Figures 10d, 10e, and 10f show the peak load, generalized stiffness (the slope of load-displacement curve), and fracture toughness of three types of granites, respectively. As the temperature increases, there is a noticeable weakening in the mechanical properties of all granite

samples, including generalized stiffness and fracture toughness. Moreover, the changes in generalized stiffness and fracture toughness with temperature follow power function trends (as shown in Figs. 10e and 10f). The fracture toughness values for CG samples at room temperature and various high temperature are lower compared to the values of MG and FG samples (Fig. 10f). For example, at 600 °C, the fracture toughness for CG, MG, and FG samples decreases by 96.4%, 88.8%, and 75.0%, respectively, from their values at 25 °C. Further increases in treatment temperature led to additional reductions in fracture toughness. At 1000 °C, the fracture toughness decreases to zero for CG sample, 0.09 $MPa \cdot m^{1/2}$ for MG sample, and 0.46 $MPa \cdot m^{1/2}$ for FG sample. The primary reason for this reduction in fracture toughness is attributed to microcracks generated by thermal damage, leading to a compromised tensile stress resistance. This phenomenon suggests a decline in the capacity of rock materials to withstand fractures as temperature increases. The interpretation of these results is supported by microscopic examination of the microcracks within the specimens, utilizing both polarization microscopy (Fig. 7) and SEM analysis (Fig. 9), aligning with findings from previous works (Akdag et al. 2020; Kang et al. 2021; Feng et al. 2021; Wang et al. 2024). Importantly, the observed variation in fracture toughness among CG samples across all examined temperature levels underscores that granites with larger average grain sizes and more heterogeneous distributions are particularly susceptible to changes in fracture toughness following exposure to high temperatures.

Fig. 10 Mechanical behavior of three types of pre-heated granites. Load-displacement curves of **a** CG samples, **b** MG samples, and **c** FG samples under different temperatures; **d** peak load, **e** generalized stiffness, and **f** fracture toughness of samples after high temperature treatment.

In addition to grain size, the mineralogical composition is recognized as a significant factor influencing the rock fracture toughness after high temperature treatment. For example, crystal transformation and mineral decomposition of aggregates can substantially affect the fracture toughness and microcracking behavior of granite. As shown in Table 1, the quartz contents in the three types of rocks are 20.1% (CG), 9.6% (MG), and 3.9% (FG), respectively. Under normal pressure conditions, trigonal quartz, also known as α-quartz or low quartz, undergoes a phase transition to hexagonal β-quartz (high quartz) at 573 °C. Subsequent heating results in the transformation of SiO_2 to hexagonal β-tridymite at 870 °C and further to cubic β-cristobalite at 1470 °C (Glover et al. 1995; Wenk and Bulakh 2004). During the temperature range studied (25~1000 °C), both the initial and

secondary phase transition of quartz maybe occurred. Consequently, the fracture toughness of the CG sample, which has the highest quartz content, exhibits a notable decline upon reaching 600 °C. Specifically, the fracture toughness of the CG samples decreases from 0.69 MPa·m$^{1/2}$ at 400 °C to 0.05 MPa·m$^{1/2}$ at 600 °C, representing a 92.7% reduction. The crystal transformation of quartz is considered an important factor leading to the deterioration of the mechanical properties of granite after high temperature treatment (Tufail et al. 2017; Kang et al. 2021; Zhang et al. 2021; Khan and Sajid 2023). Additionally, it is established that low and high albite phases remain stable below 650 °C and 725 °C, respectively, under low pressure conditions (Brown 1989). The MG and FG samples, characterized by lower quartz and higher albite contents, demonstrate greater stability at high temperatures, consistent with observed variations in mechanical properties (Fig. 10). Through the presented experimental findings and analyses, it becomes evident that grain size and mineralogical composition primarily dictate the mechanical behavior of granites subjected to high temperature conditions. Among the examined rock types, CG samples exhibit the most significant deterioration, attributed chiefly to the development of internal cracks, alongside the crystallographic transformation of quartz at high temperatures (e.g., 600 °C to 1000 °C).

The parameter of crack density serves as a crucial internal variable in micromechanics-based damage models (Shao and Rudnicki 2000; Rong et al. 2018; Hu et al. 2023d). Analyzing the relationship between crack density and the mechanical properties of rocks is crucial. It helps in understanding the process of thermal damage evolution observed in laboratory tests. Furthermore, it assists in developing a reliable method to estimate the mechanical properties of rocks subjected to high temperature treatments. The dependence of the normalized fracture toughness on treatment temperature and linear crack density (Table 2) was examined using 18 experimental datasets in this work (Fig. 11a). And the best-fitting formulation is derived:

$$\begin{cases} K_{\mathrm{IC}}^{\mathrm{Nor}} = 1.25 - 1.95\times10^{-4}T - 0.71\rho + 8.08\times10^{-7}T^2 + 0.13\rho^2 - 3.03\times10^{-4}T\rho \qquad R^2 = 0.97 \\ K_{\mathrm{IC}(T)} = K_{\mathrm{IC(rt)}} \times K_{\mathrm{IC}}^{\mathrm{Nor}} \end{cases} \tag{3}$$

where $K_{\mathrm{IC}}^{\mathrm{Nor}}$ is the normalized fracture toughness of the granite; T is the treatment temperature (range 25~1000 °C); ρ is the linear crack density (range 0.31~4.34 mm/mm^2); $K_{\mathrm{IC}(T)}$, $K_{\mathrm{IC(rt)}}$ is the fracture toughness of granite sample at the temperature T and room temperature, respectively. The coefficient of determination (R^2) for Eq. (3) is 0.97, underscoring the robustness of the proposed estimation

equation. Consequently, this enables the prediction of granite fracture toughness at various elevated temperatures using Eq. (3), leveraging fracture toughness data acquired at room temperature and linear crack density determined using optical images under these elevated thermal conditions.

Fig. 11 The relationship between crack density and rock fracture toughness under different temperatures. **a** dependence of normalized fracture toughness of the granite samples on treatment temperature and linear crack density; **b** evolution of the fracture toughness with linear crack density.

A theoretical relationship exists between crack density and rock fracture toughness (Nasseri et al. 2007). A significant reduction in fracture toughness with increasing crack density is forecasted by their model. The experimental results of this work are consistent with the theoretical model of Nasseri et al. (2007) and its experimental results for chevron cracked notched Brazilian disc (CCNBD) samples of Westerly granite (Fig. 11b). Both sets of experimental data indicate that fracture toughness is expected to decrease by at least 50% for crack densities exceedingly approximately 1.0 mm/mm², highlighting a marked reduction in rock resistance to crack propagation beyond this threshold. This understanding is crucial in engineering support systems for deep underground rock structures. Notably, the sensitivity of fracture toughness to crack density appears more pronounced in SCB tests compared to CCNBD assessments. Power function fittings to the experimental data (Fig. 11b) demonstrate a steep decline in fracture toughness with increasing crack density in SCB tests, whereas CCNBD tests show a more gradual decrease. For example, when the crack density is greater than 6.0 mm/mm^2, the fracture toughness measured by SCB samples has dropped to zero, whereas that of CCNBD samples remains around 0.43 $MPa \cdot m^{1/2}$. This difference may partly arise from different methodologies employed in measuring rock fracture toughness. For example, mode I fracture toughness of Kowloon granite measured by SCB test is much lower (56.5% lower) than the result obtained by cracked chevron notched semi-circular bend (CCNSCB) (Wong et al. 2019). Despite these methodological variances in fracture toughness assessment, both the results of this work and those of Nasseri et al. (2007) support the strong correlation between fracture toughness and crack density. Furthermore, this study reveals that the observed degradation in fracture toughness post-heating predominantly stems from an increase in crack density due to thermal stress. The CG samples, characterized by their heterogeneous grain size distribution and quartz-rich composition, exhibit heightened vulnerability to this weakening effect.

3.3. Fracture path analysis after mode I loading based on thin-section petrography

Rocks consist of mineral grains of varying size and type. The growth of fracture paths occurs along these mineral grains, resulting in IG cracks, or between the boundaries of these grains, leading to GB cracks. Consequently, the fracture paths are non-linear, and analyzing them provides valuable insights into how microstructure influences microcracking behavior. To trace the fracture paths, a series of thin-section samples was prepared using the technique illustrated in Fig. 5, followed by the acquisition and merging of multiple optical images under a microscope.

3.3.1. Fracture paths analysis of granite samples at room temperature

Analysis of the fracture path for CG, MG and FG samples at room temperature is shown in Fig. 12. Comparing Figs. 12a, 12b, and 12c reveals significant differences influenced by grain size and type. Among the samples studied, the CG sample exhibits the most tortuous fracture path (Fig. 12a), while the FG sample shows a relatively straighter path (Fig. 12c). The larger average grain size in the CG sample (Fig. 3) results in fewer minerals adjacent to the fracture path, predominantly composed of albite (Ab) and quartz (Qtz) with large sizes. Particularly, albite in the CG sample exerts a significant influence on its fracture path. As can be seen from Fig. 12a, the fracture path traverses two albite minerals with large size, with IG cracks formed thereby largely controlling the macroscopic fracture direction. Conversely, the fracture path of FG sample intersects a greater number of minerals (Fig. 12c), leading to a smoother macroscopic fracture boundary.

Fig. 12 Fracture path analysis for the CG, MG and FG samples at room temperature. Fracture path of **a** CG sample, **b** MG sample and **c** FG sample under mode I loading; **d** crack path through a biotite grain; **e** grain debris in CG sample; **f** fracture changes from step pattern to straight-line pattern due to mineralogical composition; **g** crack branching in MG sample between microcline and albite; **h** crack branching in FG sample inside albite. Qtz: quartz, Mcc: microcline, Hbl: hornblende, Bt: biotite, Ab: albite.

In addition to the variations in fracture path tortuosity, the dominant types of microcracks (GB crack or IG crack) among the three types of samples at room temperature are different. IG cracks prevail in the CG and MG samples, whereas GB cracks are more prominent in the FG sample. This observation suggests an increasing proportion of IG cracks with larger grain sizes, consistent with

findings in granite and hornfels by Alneasan and Behnia (2021). Mechanically, under mode I loading conditions, fractures are inclined to advance in a direct line from the notch tip towards the load application point, following the path of maximal tangential stress (Wei et al. 2017). This path imposes a specific propagation route for the fracture. Along this route, the fracture faces resistance from the bond strength between mineral grains as it traverses their interfaces, or from the intrinsic strength of the mineral grains themselves. If the advancing fracture encounters a large grain while progressing towards the loading point, it will deflect around the grain to stay within the stress field. In these cases, the specific grain type becomes inconsequential, as the primary determinant is adherence to the predetermined stress-induced pathway. For example, in the CG sample, cracks penetrate albite minerals to maintain the stress path (see Fig. 12a), aligning with mechanical principles. Similarly, in the MG sample, the fracture passed through quartz, albite and microcline multiple times, generating numerous IG cracks (Fig. 12b). Furthermore, when fractures encounter large grains, less energy is required to cleave the grain itself compared to rupturing bonds along grain boundaries (Alneasan and Behnia 2021). Fracture propagation through grain boundaries occurs when these boundaries align with mechanical principles, as depicted in Fig. 12c. Smaller average grain sizes and more homogeneous grain size distributions result in grain boundaries offering more pathways that are in agreement with mechanical considerations. In this study, the CG and MG samples have average grain sizes 20.39 and 9.67 times larger than those of the FG samples, respectively. The microstructure with homogeneous grain size distribution and a smaller average grain size in the FG samples provides a rich grain boundary network for crack propagation (Fig. 12c). Thus, when the path of maximum tangential stress aligns with a grain boundary, it facilitates propagation of fractures between grains.

Figure 12d shows the details of fracture passing through a biotite in the CG sample, revealing two distinct fracture paths. Firstly, the upper fracture passes through the biotite. Influenced by maximum tangential stress, the fracture path changes from parallel to the cleavage and then deflects almost perpendicular to the cleavage. Previous research has demonstrated that fracture propagation perpendicular to grain orientation results in greater roughness compared to parallel propagation along the grain axis (Nasseri et al. 2010). This seems to be consistent with the experimental observations in this work. Secondly, the lower fracture encounters the boundary between biotite and albite, aligned with the applied load direction, and proceeds through it. Two fractures split the biotite grain into several unequal segments, then merge into one main fracture and continue to expand forward to

remain in the stress path (Fig. 12d). Fig. 12e displays the formation of grain debris resulting from fracture propagation, significantly contributing to the increase in fracture surface roughness. Fig. 12f exhibits two distinct microscopic fracture morphologies resulting from intricate interactions between minerals and fractures: a step pattern perpendicular to the cleavage plane and a straight-line pattern. Clearly, the step pattern displays rougher surfaces with irregular jagged shapes compared to the smoother straight-line pattern. Furthermore, Fig. 12f highlights the crack deflection phenomenon, a response to tensile stress under mode I loading conditions, showcasing the complex nature of fracture mechanics in rock materials.

Previous studies have indicated that the bonding strength and fracture toughness at grain boundaries typically exhibit lower values compared to the tensile strength of individual mineral grains, such as quartz (Savanick and Johnson 1974). Furthermore, owing to the varied mechanical properties inherent in grain boundaries (Liu et al. 2023; Hu et al. 2024), mineral grains within crystalline rocks demonstrate considerably greater resistance to damage than the grain boundaries (Peng et al. 2023). Therefore, it seems that GB cracks are more likely to initiate than IG cracks. However, in SCB tests, due to the special specimen geometry and loading method, there is a predetermined path for crack propagation. This setup can reverse the trend, making IG cracks more likely to initiate (Wong et al. 2019). The experimental results of this work show that the grain size also has an impact on the number of two types of cracks, with a decrease in grain size correlating with an increase in IG crack formation. Another important phenomenon in the fracture propagation process is crack branching, which has also been focused on in previous studies (Zhuang et al. 2022; Mo et al. 2023; Aghababaei et al. 2024; Hu et al. 2024). Crack branching often results in rough surfaces (Figs. 12g and 12h).

3.3.2. Fracture paths analysis of granite samples after high temperature treatment

Figure 13 shows the fracture paths of MG and FG samples after high temperature treatment. Comparative analysis reveals distinct differences in fracture path tortuosity between MG samples at various temperatures (Figs. 13a and 13b). Specifically, as the treatment temperature rises from 400 °C to 800 °C, there is a marked increase in the tortuosity of MG sample fracture paths, attributed to thermally induced microcracks at elevated temperatures (Fig. 13c). These microcracks offers additional pathways for fracture propagation from the notch tip, promoting crack branching and thereby augmenting fracture path tortuosity. Fig. 13b illustrates that subsequent to initiation from the

notch tip, the fracture undergoes significant angular deviation, crossing the boundary between albite and microcline to form a GB crack. This phenomenon is linked to the previously discussed adaptation of stress path to fracture path.

Conversely, the tortuosity of fracture paths in FG samples under high temperature conditions exhibits minimal variation (Figs. 13d and 13e), with negligible differences in fracture tortuosity observed. The high temperature treatment notably increases the number of broken mineral grains (Fig. 13g), leading to significant mineral loss visible in the optical image of FG samples (Fig. 13e). This is evident when comparing the minerals on either side of the fracture in Fig. 13f, where the types and shapes of minerals do not correspond along the fracture path. Experimental findings suggest that the influence of temperature on the fracture path is notably more substantial in rocks characterized by larger average grain sizes and more heterogeneous grain size distributions. Conversely, in rocks with smaller or more homogeneous grain sizes, the impact of temperature on the fracture path appears to be minimal.

Fig. 13 Fracture path analysis for the MG and FG samples after high temperature treatment. Fracture path of MG sample at **a** 400 °C and **b** 800 °C; **c** the fracture splits the microcline grain into two unequal parts, and there are many thermally induced microcracks distributed around the main macroscopic fracture; fracture path of FG sample at **d** 400 °C and **e** 800 °C; **f** grain missing; **g** a broken hornblende grain in FG sample. Qtz: quartz, Mcc: microcline, Hbl: hornblende, Bt: biotite, Ab: albite.

To quantitatively investigate the effect of temperature on rock fracture paths, detailed analyses of MG samples at 25 °C, 400 °C, and 800 °C were conducted using ImageJ software (Fig. 14). This analysis included measurements of fracture width, actual fracture length, and nominal fracture length. Due to the inherent heterogeneity of rocks, which includes variations in both microstructural and mechanical property, a consistent discrepancy between actual and nominal fracture lengths was found. Tortuosity, defined as the square of the ratio between the nominal and actual length of the fracture path (Akhavan and Rajabipour 2012), has been widely utilized in previous studies to analyze the microcracking behavior of SCB samples (Alneasan and Behnia 2021; Aghababaei et al. 2024). Fracture width was measured at intervals of 1.0 mm along the fracture path, and the average width was subsequently calculated. The average width is an important parameter in studying the

permeability of the rocks. Many previous results show that high temperature treatment will increase the permeability of rocks (Feng et al. 2021; Kang et al. 2021). As shown in Fig. 14, the average width of fracture path increases with the increases of treatment temperature. The average widths of fracture path for MG samples at 25 °C, 400 °C and 800 °C are 0.282 mm, 0.385 mm and 0.755 mm, respectively. After being treated at 800 °C, the fracture width of the MG sample is 2.68 times higher than the measured value at room temperature. The tortuosity value of the fracture path of MG samples at 25 °C, 400 °C and 800 °C was computed and summarized in Table 3. Based on the definition of this characteristic, an increase in tortuosity leads to a closer alignment between the actual and nominal lengths, resulting in a straighter fracture path. Table 3 further illustrates a reduction in fracture path tortuosity in MG samples with increasing treatment temperature, along with an inverse relationship between tortuosity and fracture path width.

Fig. 14 Fracture path width of MG samples at **a** 25 °C, **b** 400 °C and **c** 800 °C. The value marked in the figures is the fracture path width of the current section with mm unit. When mineral loss occurs, the section is invalid. It is worth noting that the fracture width in pre-heated SCB samples was directly measured from the middle sections, as depicted in Fig. 5.

Table 3 The tortuosity of MG samples at different temperatures

From the comprehensive quantitative and qualitative analysis conducted above, it is evident that the influence of temperature on microcracking behavior intensifies with increasing grain size. Specifically, in coarse-grained rocks (e.g., CG samples in this work), the distribution of thermal stress becomes more heterogeneous with rising temperatures, resulting in a more significant accumulation of thermally induced microcracks (Fig. 7). During mode I loading, the interaction between microcracks induced by thermal stress and tensile stress contributes to the formation of a more tortuous fracture path. Additionally, the fracturing of mineral grains contributes to a rougher, zig-zag appearance along the fracture edges. In contrast, fine-grained rocks (e.g., FG samples in this work) exhibit a more homogeneous thermal stress distribution, resulting in fewer thermally induced microcracks. The smaller average grain size and more homogeneous grain size distribution in these rocks reduce the likelihood of macroscopic fractures intersecting with thermally induced cracks during propagation, resulting in fracture paths that align more closely with the direction of applied

stress. Consequently, the fracture edges in such cases are smoother, as shown in Fig. 13d. However, at very high treatment temperatures, minerals within fine-grained rocks tend to fragment into smaller particles under mode I loading conditions, creating visible voids in mineral presence within optical images (Fig. 13e), indicating a significant impact of high temperatures on rock integrity.

4. Discussion

4.1. The effect of grain-scale heterogeneity on tensile microcracking behavior

The grain-scale heterogeneity of the rock materials can significantly influence the distribution of thermal stress during heating, resulting in varying thermally induced microcrack distributions and ultimately different tensile cracking behavior under mode I loading. Grain size and mineralogical composition, key sources of grain-scale heterogeneity, have been shown in previous studies to affect the microcracking behavior of rocks under various loading conditions (Li et al. 2018; Peng et al. 2017, 2018; Zhang et al. 2018; Du et al. 2022; Hu et al. 2020, 2023b, 2023c, 2024; Inga et al. 2023; Petružálek et al. 2023; Yan et al. 2023). However, when rocks are subjected to high temperatures, these cracking behaviors may change due to the influence of the grain-scale heterogeneity (Kahraman et al. 2020; Feng et al. 2021; Yin et al. 2021; Hu et al. 2023b; Khan and Sajid 2023). For example, increasing temperatures have been observed to induce significant mineral instability, manifesting as thermally induced fractures, expansion of pre-existing cracks, carbonate mineral decomposition, and grain boundary separation (Wong et al. 2020; Khan and Sajid 2023). Nevertheless, the influence of grain size and mineralogical composition on the tensile microcracking behavior of rocks following high temperature treatment remains insufficiently investigated.

This study examined three varieties of pre-heated granites with distinct grain sizes and mineralogical compositions under mode I loading. The results indicate an inverse relationship between mode I fracture toughness and both grain size and temperature. Conversely, linear crack density shows a direct correlation with both grain size and temperature. Analysis of fracture paths reveals that a decrease in grain size leads to reduced tortuosity and a straighter path. Larger grain sizes result in fracture paths influenced by stronger and larger minerals (Fig. 13b). As the temperature increases, the fracture path in medium-grained rocks becomes more tortuous and wider (Fig. 14). Therefore, thermally induced cracks contribute to increased tortuosity in samples with larger grain

sizes (e.g., MG and CG samples). However, as grain size decreases, the effect of temperature on the fracture path appears negligible. For example, the average grain size of FG samples in this work is 0.18 mm, and the tortuosity of the fracture path in FG samples after high temperature treatment at 400 °C and 800 °C is almost identical (Fig. 13). Nonetheless, in FG samples treated at 800 °C, mineral fragmentation occurs, leading to potential mineral loss during thin-section sample preparation (Fig. 13e).

The influence of grain size on fracture paths surpasses that of mineralogical composition across varying high temperatures, aligning with previous experimental results conducted at room temperature (Jiang et al. 2017; Alneasan and Behnia 2021; Aghababaei et al. 2024). This phenomenon is attributed to grain size or its heterogeneity. In fine-grained rocks, such as FG samples, the mineralogical composition can be disregarded. However, in medium-grained and coarse-grained rocks, such as the MG and CG samples in this work, which are characterized by larger average grain sizes and more heterogeneous grain size distributions, mineralogical composition significantly affects fracture paths and can even directly alter their course (see Fig. 13b). This insight is crucial for thermo-mechanical modeling of granite, suggesting that both grain size and mineralogical composition should be integrated into numerical models for more accurate simulations. Neglecting these factors could lead to an underestimation of the effect of temperature on the tensile cracking behavior of rocks.

4.2. Implications

For practice applicability, experimental results indicate that grain size and mineralogical composition significantly affect the cracking behavior of rocks after high temperature treatment. The density of thermally induced cracks increases with grain-scale heterogeneity, such as larger average grain size and more heterogeneous grain size distribution. This finding underscores the importance of site selection for deep geothermal reservoirs at the field scale. Thermal cracking is more severe in coarse-grained rocks than in fine-grained ones, making coarse-grained granite more suitable for deep geothermal reservoir siting, as it facilitates the extraction of geothermal energy (Feng et al. 2021; Yin et al. 2021). Thermal cracking enhances reservoir permeability, facilitating heat exchange and transport crucial for geothermal exploitation. Consequently, the presence of coarse-grained granite constitutes a favorable geological base for geothermal energy utilization. Mineralogical composition influences fracture paths in medium-grained and coarse-grained rocks, shaping fracture network

distribution. Laboratory-scale mineralogical analysis can assess geothermal reservoir permeability preliminarily.

Moreover, the investigation indicates that grain size and mineralogical composition influence the fracture toughness of rocks at elevated temperatures, with grain size demonstrating a more pronounced effect. Previous studies have confirmed that grain size significantly affects rock fracture toughness at room temperatures (Alneasan and Behnia 2021; Aghababaei et al. 2024). Consequently, for deep rock engineering projects that require long-distance support design, more refined and detailed structural support design seems to be necessary. For example, in scenarios such as the depth of approximately 4 km for high-temperature deep disposals (Gibb et al. 2008), the surrounding rock type transitions progressively from fine-grained to coarse-grained, accompanied by a corresponding rise in temperature. This gradual thermal escalation diminishes the fracture toughness of the surrounding rock, necessitating progressively reinforced tunnel support with increasing depth. Neglecting the influence of grain size could lead to an overestimation of fracture toughness, potentially resulting in inadequate support design.

4.3. Limitations

In this work, 2D microscopic observation by polarization microscopy and SEM was employed to capture the microcracking behavior of three types of granite specimens with quasi-static mode I loading conditions. However, the cracking behavior of rocks may be influenced by the more complex loading conditions and geological factors in the field (Funatsu et al. 2014; Yao et al. 2020; Ma et al. 2022; Alneasan and Alzo'ubi 2023). Future work could extend the present study to other loading conditions, such as mode I loading with confining pressure and fatigue loading, in order to gain deeper insights into the complex relationship between grain-scale heterogeneity, loading conditions, temperature and cracking behavior.

The present study focuses on examining the mechanical behavior of granite subjected to high temperatures, followed by cooling at the same heating rate. Prior works has demonstrated that the cooling rate (e.g., slow cooling, water cooling, and liquid nitrogen cooling) significantly impacts the mechanical properties and microstructure of pre-heated rocks (Sha et al. 2020; Zhu et al. 2020; Shao et al. 2022; Srinivasan et al. 2022). For example, liquid nitrogen cooling induces stronger thermal shock in pre-heated rocks compared to water cooling and slow cooling, resulting in the most severe

damage to the rock microstructure (Sha et al. 2020). Future studies should therefore extend the current research by investigating different cooling conditions, including water cooling and liquid nitrogen cooling, to achieve a more comprehensive understanding of the tensile microcracking behavior of granite.

Visualizing microcrack initiation, propagation, and coalescence within rocks during heating or cooling remains challenging with current experimental techniques. Given the limitations of laboratory work, numerical simulation serves as a crucial supplementary method to validate experimental results and investigate the microcracking behavior of rocks (Peng et al. 2018; Huang et al. 2019; Saksala 2021; Hu et al. 2023b). Numerical simulations also enable precise quantitative studies of the relationship between microstructure and mechanical properties of pre-heated rocks. Existing studies have predominantly focused on the fracture processes of rocks under compressive loading (Peng et al. 2017; Hu et al. 2023b) or have overlooked the impact of temperature (Zhang et al. 2023). Few numerical studies, however, have explored the effect of microstructure on the microcrack behavior of pre-heated rocks under mode I loading. Furthermore, the low cost and high efficiency of numerical simulations make them a viable method for determining the optimal coupling conditions (stress and temperature) for crack propagation. Consequently, it is essential to investigate the tensile microcracking behavior of granites after high temperature treatment using numerical methods such as the discrete element method (DEM) or the combined finite-discrete element method (FDEM).

Furthermore, Mo et al. (2023) emphasized the importance of integrating both the fracture toughness of mineral grains and grain boundaries to accurately predict the microcrack behavior of granite. Their study revealed that the deflection angle (the angle between the direction of propagated crack and mineral cleavage) and the fracture toughness ratio (between grain boundary and mineral grain) determine whether microcracks deflect or penetrate (Chen et al. 2019; Mo et al. 2023). Incorporating these insights into future analyses will advance our comprehension of the factors influencing fracture path selection at grain-scale during crack propagation.

An empirical formulation (Eq. (3)) has been proposed to predict the mode I fracture toughness of granite subjected to different temperature treatments, explicitly considering measured linear crack density. The effectiveness of this empirical formulation was demonstrated through its strong correlation with experimental results (R^2=0.97). This simplified approach allows for the estimation of mode I fracture toughness in high temperature environments using basic experimental

measurements conducted at room temperature. The empirically-derived formulation offers guidance for site selection, design, and construction of deep geological repositories. However, in-situ geological conditions are considerably more complex than the well-controlled stress conditions in laboratory tests. Therefore, further refinement of the proposed empirical formula through additional laboratory and field data is essential.

5. Conclusions

The influence of grain size and mineralogical composition on the thermally induced cracks, fracture surface topography, fracture toughness, and fracture path among three types of granites subjected to high temperature treatment were investigated. The following conclusions are drawn:

(1) Granites with larger average grain sizes and more heterogeneous grain size distributions are more sensitive to thermal treatment. Specifically, coarse-grained granites are more likely to initiate visible macro-scale thermal cracks after high-temperature treatment. The linear thermal crack density increases with both temperature and grain size.

(2) Fracture surface topographies vary with mineralogical composition and treatment temperature. At lower temperatures (e.g., 25~200 °C), brittle shear fractures are prone to occur within quartz (e.g., conchoidal fracture). At higher temperatures (e.g., 800~1000 °C), tensile fractures are more likely to occur within feldspars (e.g., lamellar tearing crack). Furthermore, as temperature increases, more diverse fracture surface topographies appear, such as dimple and crack branching.

(3) Mode I fracture toughness of granites decreases with increasing temperature and grain size. The brittle-ductile transition is more evident in coarse-grained granites at 400 °C~600 °C, whereas fine-grained granites exhibit brittle characteristics even after treatment at 1000 °C. An empirical formulation (Eq. (3)) was proposed to predict the mode I fracture toughness of pre-heated granite by explicitly considering the linear crack density.

(4) At room temperature, granites with larger average grain sizes and more heterogeneous grain size distributions have more tortuous fracture paths and more intra-grain cracks under mode I loading. In granites with smaller average grain sizes and more homogeneous grain size distributions, longer grain boundaries provide more path options consistent with the stress path between the notch tip and the applied loading point. In medium-grained granites, the tortuosity and width of fracture paths

increase with treatment temperature. However, the effect of temperature on the tortuosity of fracture paths in fine-grained granites is negligible.

Declaration of Competing Interest

The authors declare that they have no known competing financial interests or personal relationships that could have appeared to influence the work reported in this paper.

Data Availability Statements

All data generated or analyzed during this work are included in this published paper and are available from the corresponding author on reasonable request.

Acknowledgements

This research was supported by the National Natural Science Foundation of China (51778575). The sponsorship guaranteed with basic research funds provided by Politecnico di Torino, Italy, for its financial aid in this work is also acknowledged. The authors sincerely thank Dr. Leguang Li at the School of Earth Sciences in China University of Geosciences (Wuhan) for his valuable assistance during the thin-section petrographic tests. The authors sincerely thank Dr. Yang Yang at the School of Materials Science and Engineering in Zhejiang University for her kindly help during the semi-circular bending tests. In addition, the first author wants to express his acknowledgment to the China Scholarship Council (CSC) for providing financial support to study at Politecnico di Torino, Italy.

References:

Aghababaei M, Behnia M, Aliha MRM (2024) Experimental Investigation on the Effect of Grain Size of Granitic Rocks on the Fracture Roughness and Toughness. Geomech Energy Envir 100535. https://doi.org/10.1016/j.gete.2024.100535

Akdag S, Karakus M, Nguyen GD, Taheri A (2020) Strain burst vulnerability criterion based on energy-release rate. Eng Fract Mech 237, 107232. https://doi.org/10.1016/j.engfracmech.2020.107232

Akhavan A, Rajabipour F (2012) Quantifying the effects of crack width, tortuosity, and roughness on wa ter permeability of cracked mortars. Cement Concr Res. 2012;42(2): 313–320. https://doi.org/10.1016/j.cemconres.2011.10.002

Alneasan M, Alzo'ubi AK (2023) Temperature effect on the fracture behavior of granite under three loading modes (I, I/II, and II). Rock Mech Rock Eng 56(3), 2197-2211. https://doi.org/10.1007/s00603-022-03149-3

Alneasan M, Behnia M (2021) An experimental investigation on tensile fracturing of brittle rocks by considering the effect of grain size and mineralogical composition. Int J Rock Mech Min Sci 137, 104570. https://doi.org/10.1016/j.ijrmms.2020.104570

Alneasan M, Alzo'ubi AK, Behnia M, Mughieda O (2022) Experimental observations on the effect of thermal treatment on the crack speed and mode I and II fracture toughness in brittle and ductile rocks. Theor Appl Fract Mec 121, 103525. https://doi.org/10.1016/j.tafmec.2022.103525

Armstrong RW (2015) Material grain size and crack size influences on cleavage fracturing. Philosophical Transactions of the Royal Society A: Mathematical, Physical and Engineering Sciences, 373(2038), 20140124. https://doi.org/10.1098/rsta.2014.0124

Atapour H, Mortazavi A (2018) The influence of mean grain size on unconfined compressive strength of weakly consolidated reservoir sandstones. J Petrol Sci Eng 171, 63-70. https://doi.org/10.1016/j.petrol.2018.07.029

Braunagel MJ, Griffith WA (2022) Microstructural controls on mixed mode dynamic fracture propagation in crystalline and porous granular rocks. J Geophys Res Solid Earth 127(3), e2021JB022528. https://doi.org/10.1029/2021JB022528

Breede K, Dzebisashvili K, Liu X, Falcone G (2013) A systematic review of enhanced (or engineered) geothermal systems: past, present and future. Geotherm Energy 1, 1-27. https://doi.org/10.1186/2195-9706-1-4

Brown WL (1989) Alkali feldspars: Ordering rates, phase transformations and behaviour diagrams for igneous rocks. Mineralogical Magazine, 53(369), 25–42. https://doi.org/10.1180/minmag.1989.053.369.03

Brückner LM, Dellefant F, Trepmann CA (2024) Quartz cleavage fracturing and subsequent recrystallizati on along the damage zone recording fast stress unloading. J Struct Geol 178, 105008. https://doi.org/ 10.1016/j.jsg.2023.105008

Chen YL, Ni J, Shao W, Azzam R (2012) Experimental study on the influence of temperature on the mechanical properties of granite under uniaxial compression and fatigue loading. Int J Rock Mech Min Sci. 56:62–66. https://doi.org/10.1016/j.ijrmms.2012.07.026

Chen H, Zhang C, Lu Q, Chen H, Yang Z, Wen Y (2019) A two-set order parameters phase-field modeling of crack deflection/penetration in a heterogeneous microstructure. Comput Method Appl M 347, 1085–1104. https://doi.org/10.1016/j.cma.2019.01.014

Chen Z, Sha S, Xu L, Quan J, Rong G, Jiang M (2022) Damage evaluation and statistic constitutive model of high-temperature granites subjected to liquid nitrogen cold shock. Rock Mech Rock Eng 55(4), 2299-2321. https://doi.org/10.1007/s00603-022-02779-x

Chon CM, Kim SA, Moon HS (2003) Crystal structures of biotite at high temperatures and of heat-treat ed biotite using neutron powder diffraction. Clay Clay Miner 51(51):519–28. https://doi.org/10.1346/C CMN.2003.0510506

Du K, Sun Y, Zhou J, Khandelwal M, Gong F (2022) Mineral composition and grain size effects on the fracture and acoustic emission (AE) characteristics of rocks under compressive and tensile stress. Rock Mech Rock Eng 55(10), 6445-6474. https://doi.org/10.1007/s00603-022-02980-y

Fei Y (1995) Thermal expansion. In: Ahrens TJ (ed) Mineral physics and crystallography: a handbook of physical constants. AGU, pp 29–44.

Feng G, Wang X, Kang Y, Zhang Z (2020) Effect of thermal cycling-dependent cracks on physical and mechanical properties of granite for enhanced geothermal system. Int J Rock Mech Min Sci 134: 104476. https://doi.org/10.1016/j.ijrmms.2020.104476

Feng ZJ, Zhao YS, Liu DN (2021) Permeability evolution of thermally cracked granite with different grain sizes. Rock Mech Rock Eng 54(4):1953–1967. https://doi.org/10.1007/s00603-020-02361-3

Funatsu T, Kuruppu M, Matsui K (2014) Effects of temperature and confining pressure on mixed-mode (I–II) and mode II fracture toughness of Kimachi sandstone. Int J Rock Mech Min Sci 67, 1-8. https://doi.org/10.1016/j.ijrmms.2013.12.009

Gallup DL (2009) Production engineering in geothermal technology: a review. Geothermics 38:326–334. https://doi.org/10.1016/j.geothermics.2009.03.001

Gao W, Dai S, Xiao T, He T (2017) Failure process of rock slopes with cracks based on the fracture mechanics method. Eng Geol 231, 190-199. https://doi.org/10.1016/j.enggeo.2017.10.020

Gao Y, Yu Z, Chen W, Yin Q, Wu J, Wang W (2023) Recognition of rock materials after high-temperature deterioration based on SEM images via deep learning. J Mater Res Technol 25:273-284. https://doi.org/10.1016/j.jmrt.2023.05.271

Gibb FG (2000) A new scheme for the very deep geological disposal of high-level radioactive waste. J Geol Soc 157(1), 27-36. https://doi.org/10.1144/jgs.157.1.27

Gibb FG, Travis KP, McTaggart NA, Burley D (2008) A model for heat flow in deep borehole disposals of high-level nuclear waste. J Geophys Res Solid Earth 113(B5). https://doi.org/10.1029/2007JB005081

Glover PWJ, Baud P, Darot M, Meredith PG, Boon SA, LeRavalec M (1995) α/β phase transition in quartz monitored using acoustic emissions. Geophys J Int 120(3):775–82. https://doi.org/10.1111/j.1365-246X.1995.tb01852.x

Griffiths L, Heap MJ, Baud P, Schmittbuhl J (2017) Quantification of microcrack characteristics and impl ications for stiffness and strength of granite. Int J Rock Mech Min Sci 100, 138-150. https://doi.org/10.1016/j.ijrmms.2017.10.013

Guéguen Y, Boutéca M (eds) (2004) Mechanics of fluid-saturated rocks. Elsevier, Amsterdam.

Guo TY, Wong LNY (2020) Microcracking behavior of three granites under mode I loading: Insights from acoustic emission. Eng Geol 278, 105823. https://doi.org/10.1016/j.enggeo.2020.105823

Guo TY, Zhao Q (2022) Acoustic emission characteristics during the microcracking processes of granite, marble and sandstone under mode I loading. Rock Mech Rock Eng 55(9), 5467-5489. https://doi.org/10.1007/s00603-022-02937-1

Heuze FE (1983) High-temperature mechanical, physical and thermal properties of granitic rocks—a review. In Int J Rock Mech Min Sci Geomech Abstr 20:3-10. https://doi.org/10.1016/0148-9062(83)91609-1

Hu X, Xie N, Zhu Q, Chen L, Li P (2020) Modeling damage evolution in heterogeneous granite using digital image-based grain-based model. Rock Mech Rock Eng 53(11), 4925-4945. https://doi.org/10.1007/s00603-020-02191-3

Hu X, Shentu J, Xie N, Huang Y, Lei G, Hu H, Gong X (2023a) Predicting triaxial compressive strength of high-temperature treated rock using machine learning techniques. J Rock Mech Geotech Eng 15(8), 2072-2082. https://doi.org/10.1016/j.jrmge.2022.10.014

Hu X, Hu H, Xie N, Huang Y, Guo P, Gong X (2023b) The effect of grain size heterogeneity on mechanical and

microcracking behavior of pre-heated Lac du Bonnet granite using a grain-based model. Rock Mech Rock Eng 56:5923-5954. https://doi.org/10.1007/s00603-023-03381-5

Hu X, Guo P, Xie N, Hu H, Lei G, Ma J, Gong, X (2023c) Creep behavior and associated acoustic characteristics of heterogeneous granite containing a single pre-existing flaw using a grain-based parallel-bonded stress corrosion model. Rock Mech Rock Eng 56:4799–4832. https://doi.org/10.1007/s00603-023-03291-6

Hu X, Qi Y, Hu H, Lei G, Xie N, Gong X (2023d) A micromechanical-based failure criterion for rocks after high-temperature treatment. Eng Fract Mech 284, 109275. https://doi.org/10.1016/j.engfracmech.2023.109275

Hu X, Liao D, Hu H, Xie S, Xie N, Gong X (2024) The influence of mechanical heterogeneity of grain boundary on mechanical and microcracking behavior of granite under mode I loading using a grain-based model. Rock Mech Rock Eng 1-31. https://doi.org/10.1007/s00603-023-03752-y

Huang L, Liu J, Zhang F, Dontsov E, Damjanac B (2019) Exploring the influence of rock inherent heterogeneity and grain size on hydraulic fracturing using discrete element modeling. Int J Solids Struct 176, 207-220. https://doi.org/10.1016/j.ijsolstr.2019.06.018

Inga CEC, Sinha S, Walton G, Holley E (2023) Modeling Brazilian tensile strength tests on a brittle rock using deterministic, semi-deterministic, and Voronoi bonded block models. Rock Mech Rock Eng 1-21. https://doi.org/10.1007/s00603-023-03329-9

Jiang C, Zhao GF, Khalili N (2017) On crack propagation in brittle material using the distinct lattice spring model. Int J Solids Struct 118, 41-57. https://doi.org/10.1016/j.ijsolstr.2017.04.024

Kahraman S, Canpolat AN, Fener M (2020) The influence of microwave treatment on the compressive a nd tensile strength of igneous rocks. Int J Rock Mech Min Sci 129, 104303. https://doi.org/10.1016/j.ijrmms.2020.104303

Kang F, Tang CA Li, Y (2021) Grain size heterogeneity controls strengthening to weakening of granite over high-temperature treatment. Int J Rock Mech Min Sci 145, 104848. https://doi.org/10.1016/j.ijrmms.2021.104848

Kataoka M, Obara Y, Kuruppu M (2015) Estimation of fracture toughness of anisotropic rocks by semi-c ircular bend (SCB) tests under water vapor pressure. Rock Mech Rock Eng 48, 1353-1367. https://doi.org/10.1007/s00603-014-0665-y

Khan H, Sajid M (2023) Investigating the textural and physico-mechanical response of granites to heat treatment. Int J Rock Mech Min Sci 161, 105281. https://doi.org/10.1016/j.ijrmms.2022.105281

Kranz RL (1983) Microcracks in rocks: a review. Tectonophysics 100(1-3), 449-480. https://doi.org/10.1016/0040-1951(83)90198-1

Kumari WGP, Beaumont DM, Ranjith PG, Perera MSA, Avanthi Isaka, BL, Khandelwal M (2019) An experimental study on tensile characteristics of granite rocks exposed to different high-temperature treatments. Geomech Geophys Geo 5, 47-64. https://doi.org/10.1007/s40948-018-0098-2

Kuruppu MD, Chong KP (2012) Fracture toughness testing of brittle materials using semi-circular bend (SCB) specimen. Eng Fract Mech 91, 133-150. https://doi.org/10.1016/j.engfracmech.2012.01.013

Lamberson L, Ramesh KT (2015) Spatial and temporal evolution of dynamic damage in single crystal α-quartz. Mech Mater 87:61–79. https://doi.org/10.1016/j.mechmat.2015.04.003

Lan H, Martin CD, Hu B (2010) Effect of heterogeneity of brittle rock on micromechanical extensile be havior during compression loading. J Geophys Res Solid Earth 115(B01202):1–14. https://doi.org/10.1029/2009JB006496

Le Maitre, RW, Streckeisen A, Zanettin B, Le Bas, MJ, Bonin B, Bateman P (Eds.) (2005) Igneous rocks: a classification and glossary of terms: recommendations of the International Union of Geological Sciences Subcommission on the Systematics of Igneous Rocks. Cambridge University Press.

Li XF, Li X, Li HB, Zhang QB, Zhao J (2018) Dynamic tensile behaviours of heterogeneous rocks: the grain scale fracturing characteristics on strength and fragmentation. Int J Impact Eng 118:98–118. https://doi.org/10.1016/j.ijimpeng.2018.04.006

Liu XY, Xu DP, Li SJ, Qiu SL, Jiang Q (2023). An insight into the mechanical and fracture characterization of minerals and mineral interfaces in granite using nanoindentation and micro X-ray computed tomography. Rock Mech Rock Eng 1–17. https://doi.org/10.1007/s00603-023-03221-6

Ma J, Li D, Zhu Q. Liu M, Wan Q (2022) The mode I fatigue fracture of fine-grained quartz-diorite under coupled static loading and dynamic disturbance. Theor Appl Fract Mec 117, 103140. https://doi.org/10.1016/j.tafmec.2021.103140

Ma X, Wang G, Hu D, Liu Y, Zhou H, Liu F (2020) Mechanical properties of granite under real-time high temperature and three-dimensional stress. Int J Rock Mech Min Sci 136, 104521. https://doi.org/10.1016/j.ijrmms.2020.104521

Mahanta B, Singh TN, Ranjith PG (2016) Influence of thermal treatment on mode I fracture toughness of certain Indian rocks. Eng Geol 210, 103-114. https://doi.org/10.1016/j.enggeo.2016.06.008

Mo C, Zhao J, Zhang D (2023) Mode I microscopic cracking process of granite considering the criticality of failure. J Geophys Res Solid Earth 128(10), e2023JB027040. https://doi.org/10.1029/2023JB027040

Nasseri MHB, Grasselli G, Mohanty B (2010) Fracture toughness and fracture roughness in anisotropic granitic

rocks. Rock Mech Rock Eng 43(4):403–415. https://doi.org/10.1007/s00603-009-0071-z

Nasseri MHB, Schubnel A, Young RP (2007) Coupled evolutions of fracture toughness and elastic wave velocities at high crack density in thermally treated Westerly granite. Int J Rock Mech Min Sci 44(4), 601-616. https://doi.org/10.1016/j.ijrmms.2006.09.008

Olasolo P, Juárez MC, Morales MP, Liarte IA (2016) Enhanced geothermal systems (EGS): a review. Renew Sustain Energy Rev 56:133–144. https://doi.org/10.1016/j.rser.2015.11.031

Peng J, Wong LNY, Teh CI (2017) Influence of grain size heterogeneity on strength and microcracking behavior of crystalline rocks. J Geophys Res Solid Earth 122(2):1054–1073. https://doi.org/10.1002/2016JB013469

Peng J, Wong LNY, Teh CI, Li Z (2018) Modeling micro-cracking behavior of Bukit Timah granite using grain-based model. Rock Mech Rock Eng 51(1):135–154. https://doi.org/10.1007/s00603-017-1316-x

Peng K, Lv H, Zou Q, Wen Z, Zhang Y (2020) Evolutionary characteristics of mode-I fracture toughness and fracture energy in granite from different burial depths under high-temperature effect. Eng Fract Mech 239, 107306. https://doi.org/10.1016/j.engfracmech.2020.107306

Peng Y, Zhang T, Yu L, Li J, Gao Y, Tian W (2023) Numerical investigation on the effect of intergranular contact bonding strength on the mechanical properties of granite using PFC3D-GBM. Int J Numer Anal Met Geomech 47(5), 694-716. https://doi.org/10.1002/nag.3488

Petružálek M, Jechumtálová Z, Lokajíček T, Kolář P, Šílený J (2023) Micro-fracturing in granitic rocks d uring uniaxial loading: the role of grain size heterogeneity. Rock Mech Rock Eng 1-19. https://doi.org/10.1007/s00603-023-03668-7

Ranjith PG, Viete DR, Chen BJ, Perera MSA (2012) Transformation plasticity and the effect of temperat ure on the mechanical behaviour of Hawkesbury sandstone at atmospheric pressure. Eng Geol 151, 1 20-127. https://doi.org/10.1016/j.enggeo.2012.09.007

Rong G, Peng J, Yao M, Jiang Q, Wong LNY (2018) Effects of specimen size and thermal-damage on physical and mechanical behavior of a fine-grained marble. Eng Geol 232, 46-55. https://doi.org/10.1016/j.enggeo.2017.11.011

Sabri M, Ghazvinian A, Nejati HR (2016) Effect of particle size heterogeneity on fracture toughness and failure mechanism of rocks. Int J Rock Mech Min Sci 81, 79-85. https://doi.org/10.1016/j.ijrmms.2015.11.002

Saksala T (2021) Numerical modeling of thermo-mechanical failure processes in granitic rock with polygonal finite elements. Int J Numer Anal Met Geom 45(13), 1900-1919. https://doi.org/10.1002/nag.3247

Savanick GA, Johnson DI (1974) Measurements of the strength of grain boundaries in rock. In Int J Rock Mech

Min Sci Geomech Abstr 11(5): 173-180. https://doi.org/10.1016/0148-9062(74)90884-5

Sha S, Rong G, Chen Z, Li B, Zhang Z (2020) Experimental evaluation of physical and mechanical properties of geothermal reservoir rock after different cooling treatments. Rock Mech Rock Eng 53:4967-4991. https://doi.org/10.1007/s00603-020-02200-5

Shao Z, Sun L, Aboayanah KR, Liu Q, Grasselli G (2022) Investigate the mode I fracture characteristics of granite after heating/-LN2 cooling treatments. Rock Mech Rock Eng 55 4477-4496. https://doi.org/10.1007/s00603-022-02893-w

Shao JF, Rudnicki JW (2000) A microcrack-based continuous damage model for brittle geomaterials. Mech Mater 32(10), 607-619. https://doi.org/10.1016/S0167-6636(00)00024-7

Shao S, Wasantha PL, Ranjith PG, Chen BK (2014) Effect of cooling rate on the mechanical behavior o f heated Strathbogie granite with different grain sizes. Int J Rock Mech Min Sci 70, 381-387. https://doi.org/10.1016/j.ijrmms.2014.04.003

Siegesmund S, Mosch S, Scheffzük C, Nikolayev DI (2008) The bowing potential of granitic rocks: rock fabrics, thermal properties and residual strain. Environ Geol 55 (7), 1437–1448. https://doi.org/10.1007/s00254-007-1094-y

Srinivasan V, Hasainar H, Singh TN (2022) Experimental study on failure and fracturing attributes of granite after thermal treatments with different cooling conditions. Eng Geol 310, 106867. https://doi.org/10.1016/j.enggeo.2022.106867

Sun Q, Zhang W, Zhu Y, Huang Z (2019) Effect of high temperatures on the thermal properties of granite. Rock Mech Rock Eng 52, 2691-2699. https://doi.org/10.1007/s00603-019-1733-0

Sun H, Sun Q, Deng W, Zhang W, Lü C (2017) Temperature effect on microstructure and P-wave propagation in Linyi sandstone. Appl Therm Eng 115, 913-922. https://doi.org/10.1016/j.applthermaleng.2017.01.026

Tribaudino M, Angel RJ, Cámara F, Nestola F, Pasqual D, Margiolaki I (2010) Thermal expansion of plagioclase feldspars. Contrib Mineral Petr 160, 899-908. https://doi.org/10.1007/s00410-010-0513-3

Tufail M, Shahzada K, Gencturk B, Wei J (2017) Effect of elevated temperature on mechanical propertie s of limestone, quartzite and granite concrete. Int J Concr Struct Mater 11(1), 17-28. https://doi.org/10.1007/s40069-016-0175-2

Vazquez P, Benavente D, Montiel D, Gomez-Heras M (2021) Mineralogical transformations in granitoids during heating at fire-related temperatures. Appl Sci 12(1), 188. https://doi.org/10.3390/app12010188

Wang J, Chen L, Su R, Zhao X (2018) The Beishan underground research laboratory for geological disposal of high-

level radioactive waste in China: planning, site selection, site characterization and in situ tests. J Rock Mech Geotech Eng 10(3):411–435. https://doi.org/10.1016/j.jrmge.2018.03.002

Wang H, Zhou L, Zhu Z, Chen J, Ma L, Shui X, Peng T (2024) Investigation of fracture characteristics of cracked granite suffered from different thermal treatments and water-cooling time. J Mater Res Technol 29:286-302. https://doi.org/10.1016/j.jmrt.2024.01.060

Wei MD, Dai F, Xu NW, Liu Y, Zhao T (2017) Fracture prediction of rocks under mode I and mode II loading using the generalized maximum tangential strain criterion. Eng Fract Mech 186, 21-38. https://doi.org/10.1016/j.engfracmech.2017.09.026

Wenk HR, Bulakh A (2004) Minerals: Their constitution and origin. Cambridge: Cambridge University Press.

Wong TF, Brace WF (1979) Thermal expansion of rocks: some measurements at high pressure. Tectonophysics 57:95–117. https://doi.org/10.1016/0040-1951(79)90143-4

Wong LNY, Guo TY, Lam WK, Ng JYH (2019) Experimental study of cracking characteristics of Kowloon granite based on three mode I fracture toughness methods. Rock Mech Rock Eng 52, 4217-4235. https://doi.org/10.1007/s00603-019-01882-w

Wong LNY, Zhang Y, Wu Z (2020) Rock strengthening or weakening upon heating in the mild temperature range? Eng Geol 272, 105619. https://doi.org/10.1016/j.enggeo.2020.105619

Wong LNY, Zhang Y, Cui X, Wu Z (2023) Thermal effect on rock strength: strengthening-weakening transition explored by grain-based model. Acta Geotech 1-16. https://doi.org/10.1007/s11440-023-02049-2

Wu X, Huang Z, Song H, Zhang S, Cheng Z, Li R, Dai X (2019) Variations of physical and mechanical properties of heated granite after rapid cooling with liquid nitrogen. Rock Mech Rock Eng 52, 2123-2139. https://doi.org/10.1007/s00603-018-1727-3

Xu XL, Karakus M (2018) A coupled thermo-mechanical damage model for granite. Int J Rock Mech Min Sci 103:195–204. https://doi.org/10.1016/j.ijrmms.2018.01.030

Yan D, Zhao L, Wang Y, Zhang Y, Cai Z, Song X, Geng J (2023) Heterogeneity indexes of unconventional reservoir shales: Quantitatively characterizing mechanical properties and failure behaviors. Int J Rock Mech Min Sci 171, 105577. https://doi.org/10.1016/j.ijrmms.2023.105577

Yang F, Santosh M, Kim SW, Zhou H (2021) Late Neoarchean to Paleoproterozoic arc magmatism in the Shandong Peninsula, North China Craton and its tectonic implications. Precambrian Res 358, 106188. https://doi.org/10.1016/j.precamres.2021.106188

Yang SQ, Ranjith PG, Jing HW, Tian WL, Ju Y (2017) An experimental investigation on thermal damage and failure

mechanical behavior of granite after exposure to different high temperature treatments. Geothermics 65, 180-197. https://doi.org/10.1016/j.geothermics.2016.09.008

Yang Y, Zhang N, Wang J (2022) Study on the effect of negative temperature change on the fracture morphology of granite under impact. Geofluids 2022. https://doi.org/10.1155/2022/4918680

Yao W, Xu Y, Xia K, Wang S (2020) Dynamic mode II fracture toughness of rocks subjected to confining pressure. Rock Mech Rock Eng 53, 569-586. https://doi.org/10.1007/s00603-019-01929-y

Yin W, Feng Z, Zhao Y (2021) Effect of grain size on the mechanical behaviour of granite under high temperature and triaxial stresses. Rock Mech Rock Eng 54, 745-758. https://doi.org/10.1007/s00603-020-02303-z

Yu M, Wei C, Niu L, Li S, Yu Y (2018) Calculation for tensile strength and fracture toughness of grani te with three kinds of grain sizes using three-point-bending test. PloS one 13(3), e0180880. https://doi.org/10.1371/journal.pone.0180880

Zhang S, Qiu S, Li P, Kou Y, Xie Z, Jia L (2023) Mode I fracture behavior of heterogeneous granite: Insights from grain-based FDEM modelling. Eng Fract Mech 284, 109267. https://doi.org/10.1016/j.engfracmech.2023.109267

Zhang H, Sun Q, Jia H, Dong Z, Luo T (2021) Effects of high-temperature thermal treatment on the porosity of red sandstone: an NMR analysis. Acta Geophys 69, 113-124. https://doi.org/10.1007/s11600-020-00526-w

Zhang ZX (2002) An empirical relation between mode I fracture toughness and the tensile strength of rock. Int J Rock Mech Min Sci 39(3), 401-406. https://doi.org/10.1016/S1365-1609(02)00032-1

Zhang Y, Wong LNY, Chan KK (2019) An extended grain-based model accounting for microstructures in rock deformation. J Geophys Res Solid Earth 124(1), 125-148. https://doi.org/10.1029/2018JB016165

Zhao Z, Liu Z, Pu H, Li X (2018) Effect of thermal treatment on Brazilian tensile strength of granites with different grain size distributions. Rock Mech Rock Eng 51, 1293-1303. https://doi.org/10.1007/s00603-018-1404-6

Zhou XP, Li GQ, Ma HC (2020) Real-time experiment investigations on the coupled thermomechanical and cracking behaviors in granite containing three pre-existing fissures. Eng Fract Mech 224, 106797. https://doi.org/10.1016/j.engfracmech.2019.106797

Zhu GQ, Feng XT, Pan PZ, Zhou YY, Yang CX, Li ZW, Taiwakuli Y (2022) Real-time monitoring of the development of brittle fracture in hard rock tunnels based on physical model test. Tunn Undergr Sp Tech 119, 104240. https://doi.org/10.1016/j.tust.2021.104240

Zhu D, Jing H, Yin Q, Ding S, Zhang J (2020) Mechanical characteristics of granite after heating and water-cooling cycles. Rock Mech Rock Eng 53, 2015-2025. https://doi.org/10.1007/s00603-019-01991-

6

Zhuang L, Zang A, Jung S (2022) Grain-scale analysis of fracture paths from high-cycle hydraulic fatigue experiments in granites and sandstone. Int J Rock Mech Min Sci 157, 105177. https://doi.org/10.1016/j.ijrmms.2022.105177

Zuo JP, Wang JT, Sun YJ, Chen Y, Jiang GH, Li, YH (2017) Effects of thermal treatment on fracture characteristics of granite from Beishan, a possible high-level radioactive waste disposal site in China. Eng Fract Mech 182, 425-437. https://doi.org/10.1016/j.engfracmech.2017.04.043

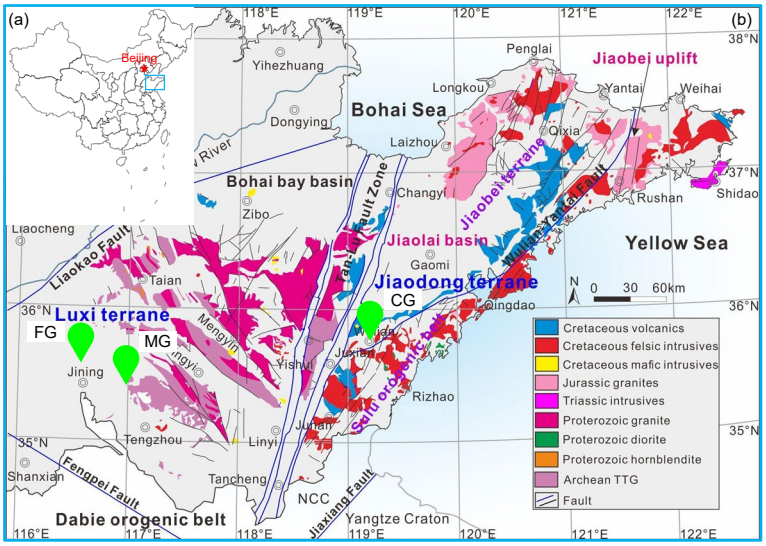

Fig. 1 Schematic geological maps of the study areas with sample localities. **a** geographical position of the study area in China; **b** geological sketch map of Shandong Peninsula (after Yang et al. 2021). Note: green points in (**b**) show location of three studied granites.

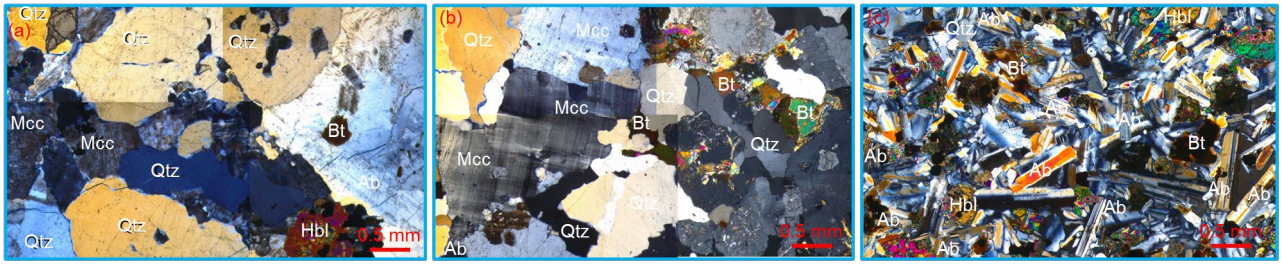

Fig. 2 Thin section of three types granites. **a** coarse-grained granite (CG); **b** medium-grained granite (MG); **c** fine-grained granite (FG). Qtz: quartz, Mcc: microcline, Hbl: hornblende, Bt: biotite, Ab: albite.

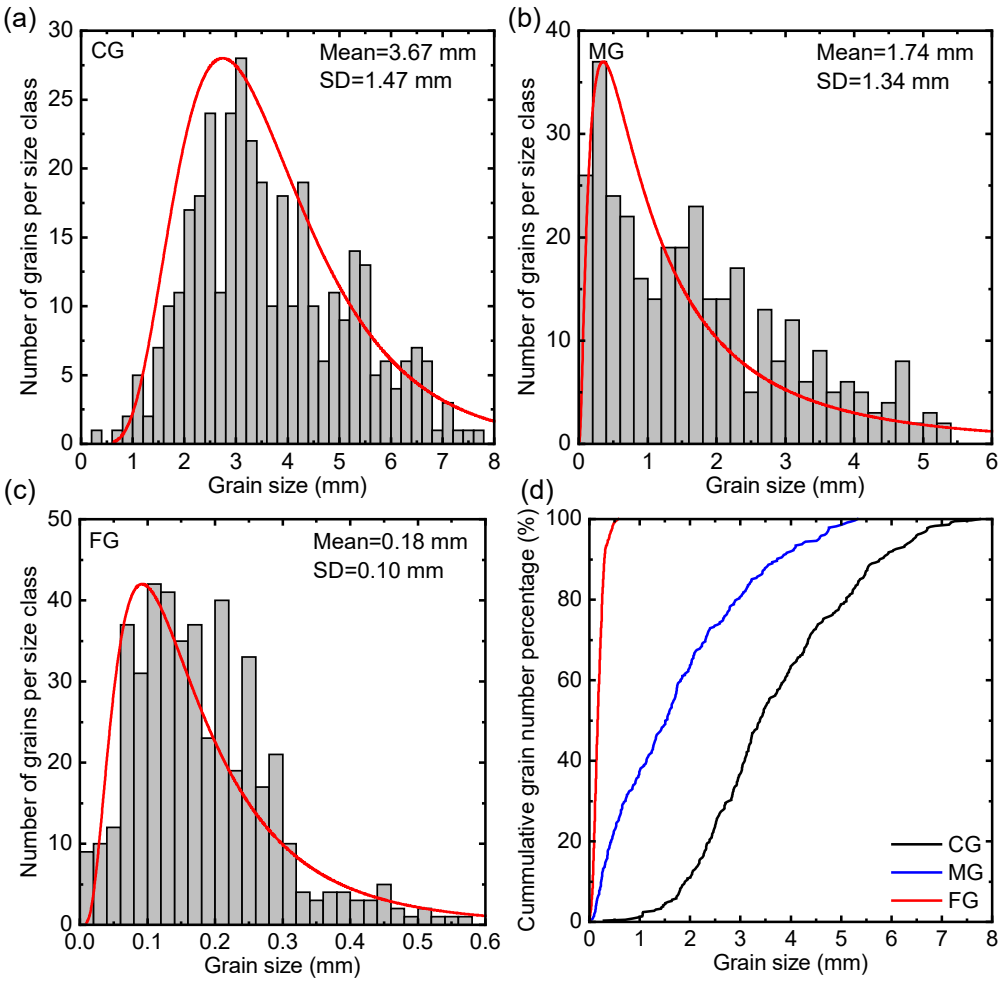

Fig. 3 Grain size distribution of three granite samples. **a** CG; **b** MG; **c** FG; **d** cumulative grain size distributions of samples. The red curves in (**a**), (**b**) and (**c**) represent the log-normal fitting curves of the grain size distribution. SD: standard deviation.

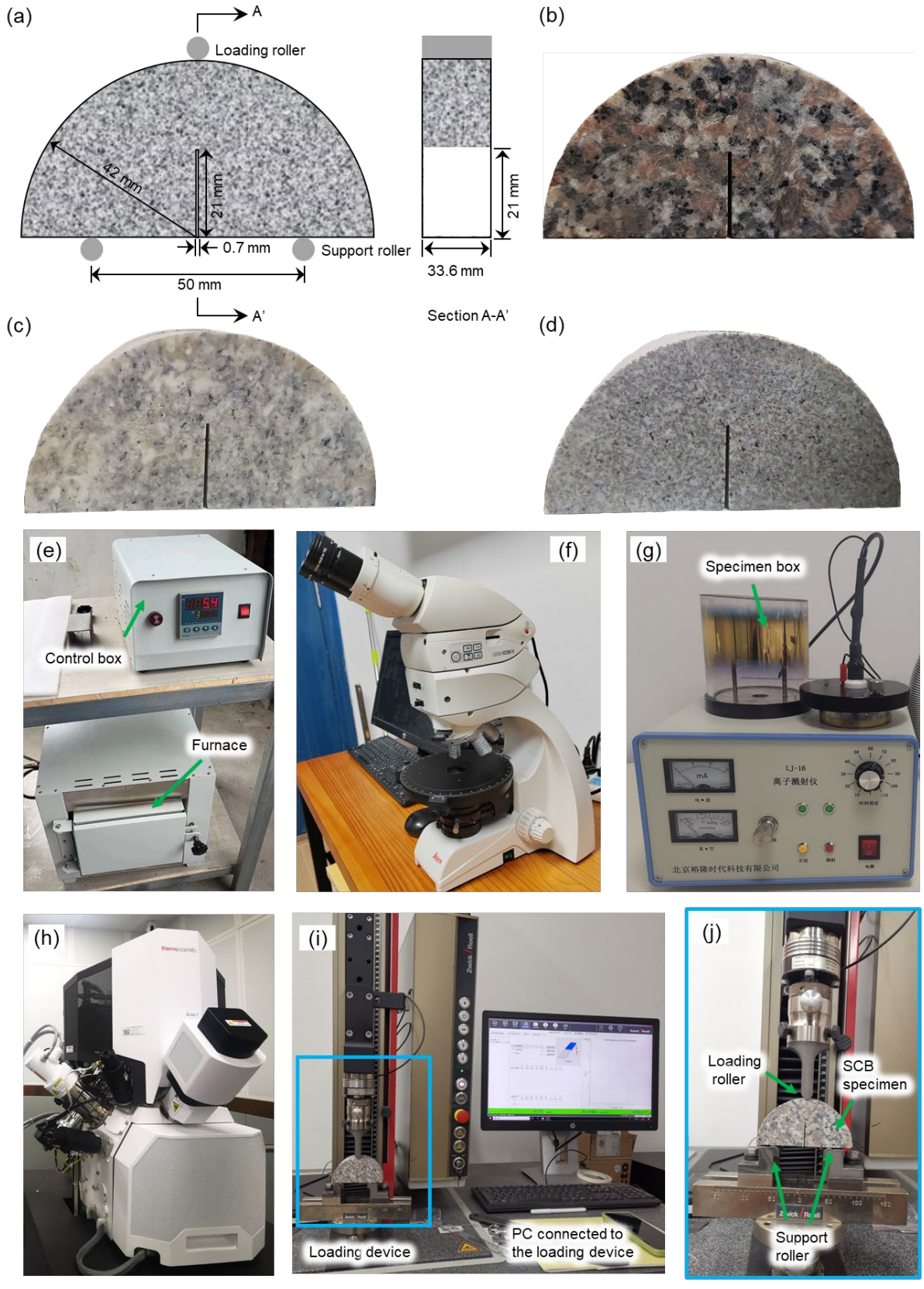

Fig. 4 Experimental study. **a** geometry of semi-circular bend specimen; **b** CG specimen; **c** MG specimen; **d** FG specimen; **e** muffle furnace; **f** Leica DM750P polarization microscopy; **g** LJ-16 ion sputtering instrument; **h** Thermo Scientific Scios 2 scanning electron microscopy; **i** universal testing machine; **j** detailed position of SCB specimen.

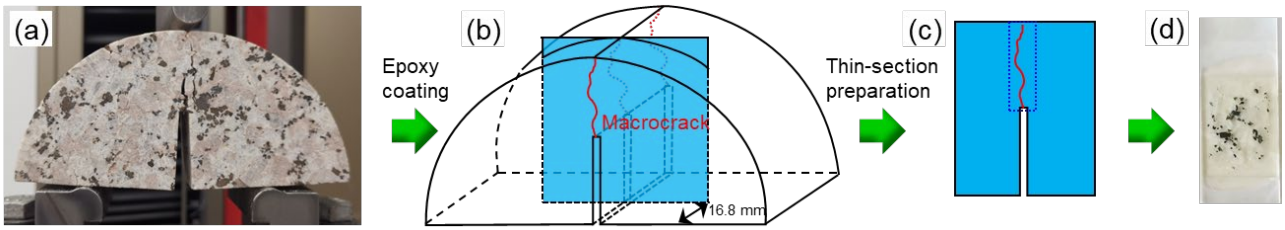

Fig. 5 Preparation procedures of the thin-section samples containing the macroscopic fracture. **a** failed sample under mode I loading; **b** position of thin-section sample; **c** region of interest; **d** thin-section sample for polarizing microscopy observation.

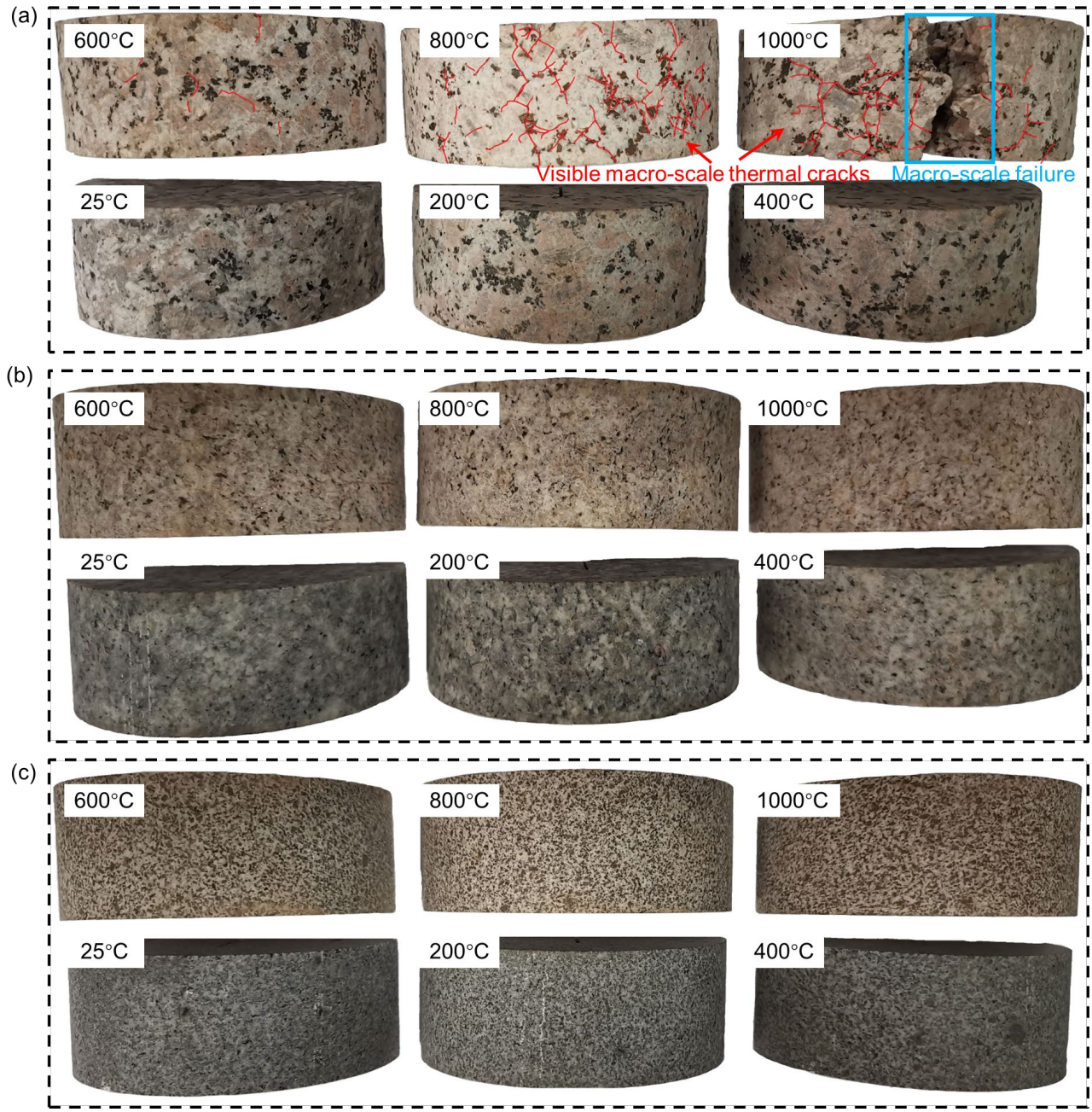

Fig. 6 Appearance of three types of granite specimens after high temperature treatment. **a** CG specimens; **b** MG specimens; **c** FG specimens.

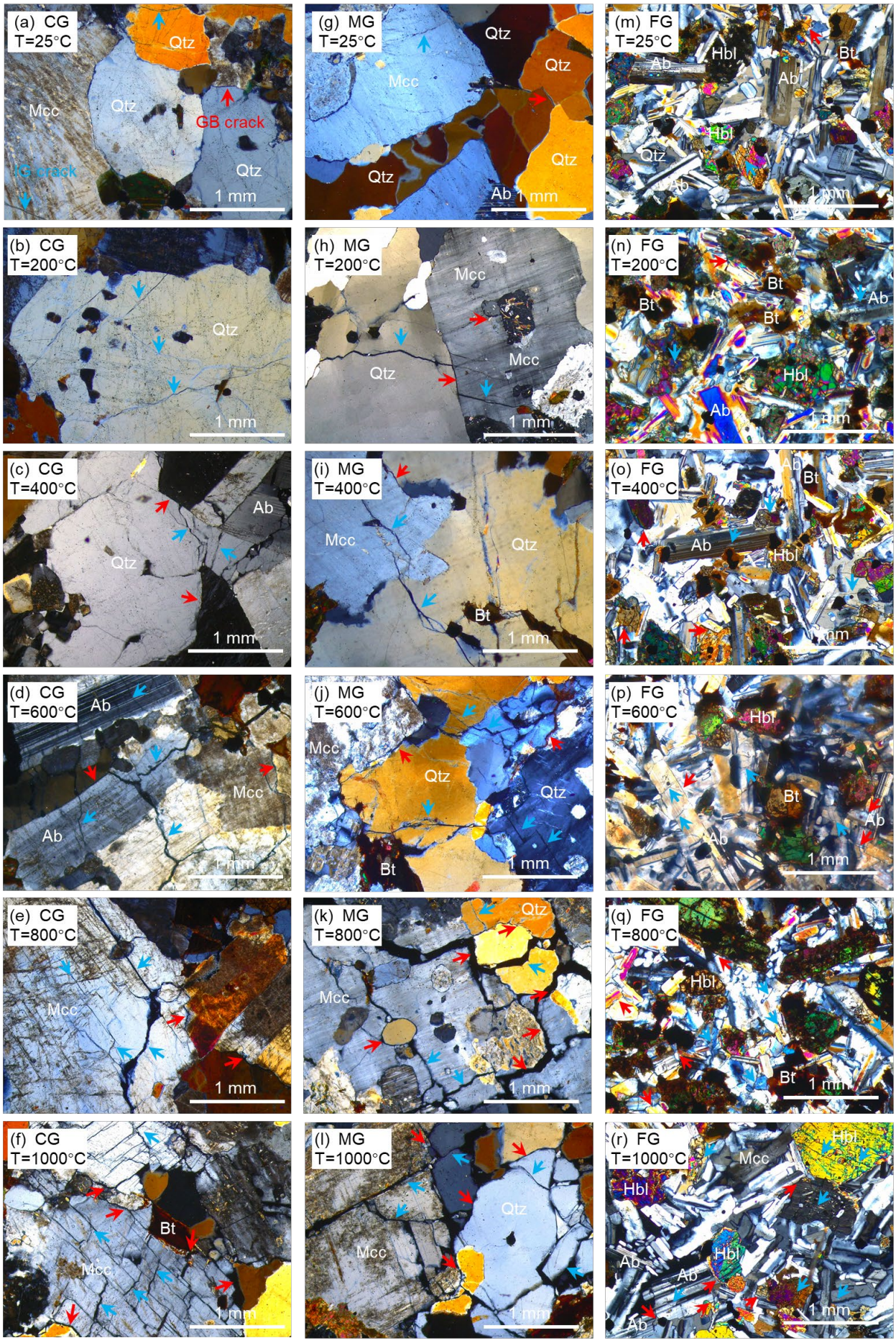

Fig. 7 The representative thin-section images of the three types of granites after high temperature

treatment. Red arrows indicate grain-boundary (GB) cracks and pure blue arrows indicate intra-grain (IG) cracks. Qtz: quartz, Mcc: microcline, Hbl: hornblende, Bt: biotite, Ab: albite.

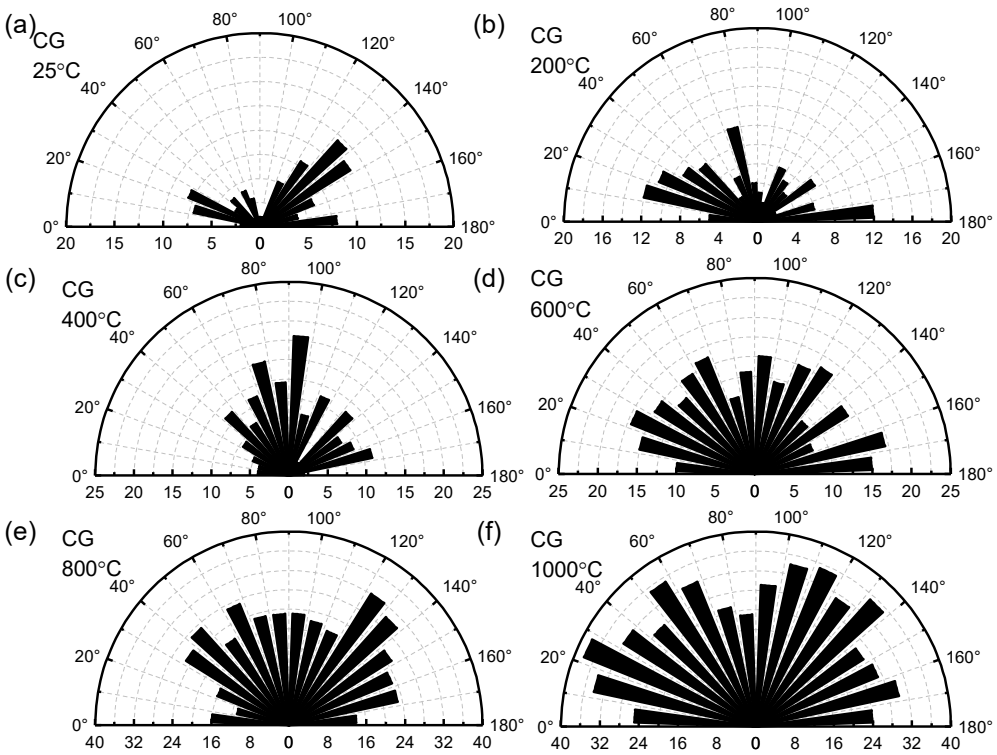

Fig. 8 The orientation distribution of thermally induced cracks within CG samples.

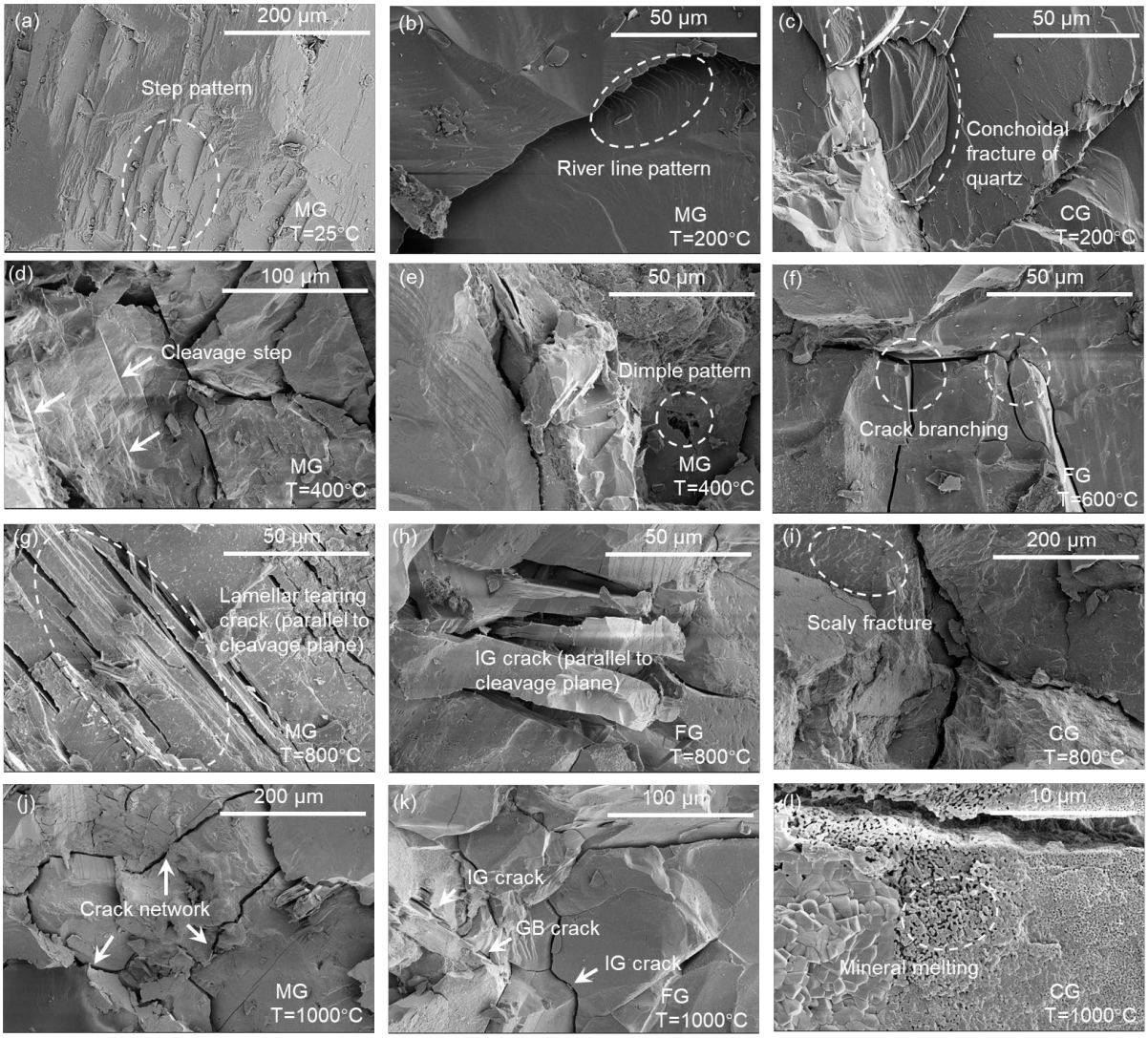

Fig. 9 Scanning electron microscope micrographs of fracture surface topography of granites under different temperatures. **a** step pattern; **b** river line pattern; **c** conchoidal fracture of quartz; **d** cleavage step; **e** dimple pattern; **f** crack branching; **g** lamellar tearing crack; **h** IG crack parallel to cleavage plane; **i** scaly fracture; **j** crack network; **k** two IG cracks connected by a GB crack; **l** mineral melting after 1000 °C treatment. Note: The areas shown were chosen independently of the evolution of the fracture process, and do not necessarily correspond to a specific failure pattern.

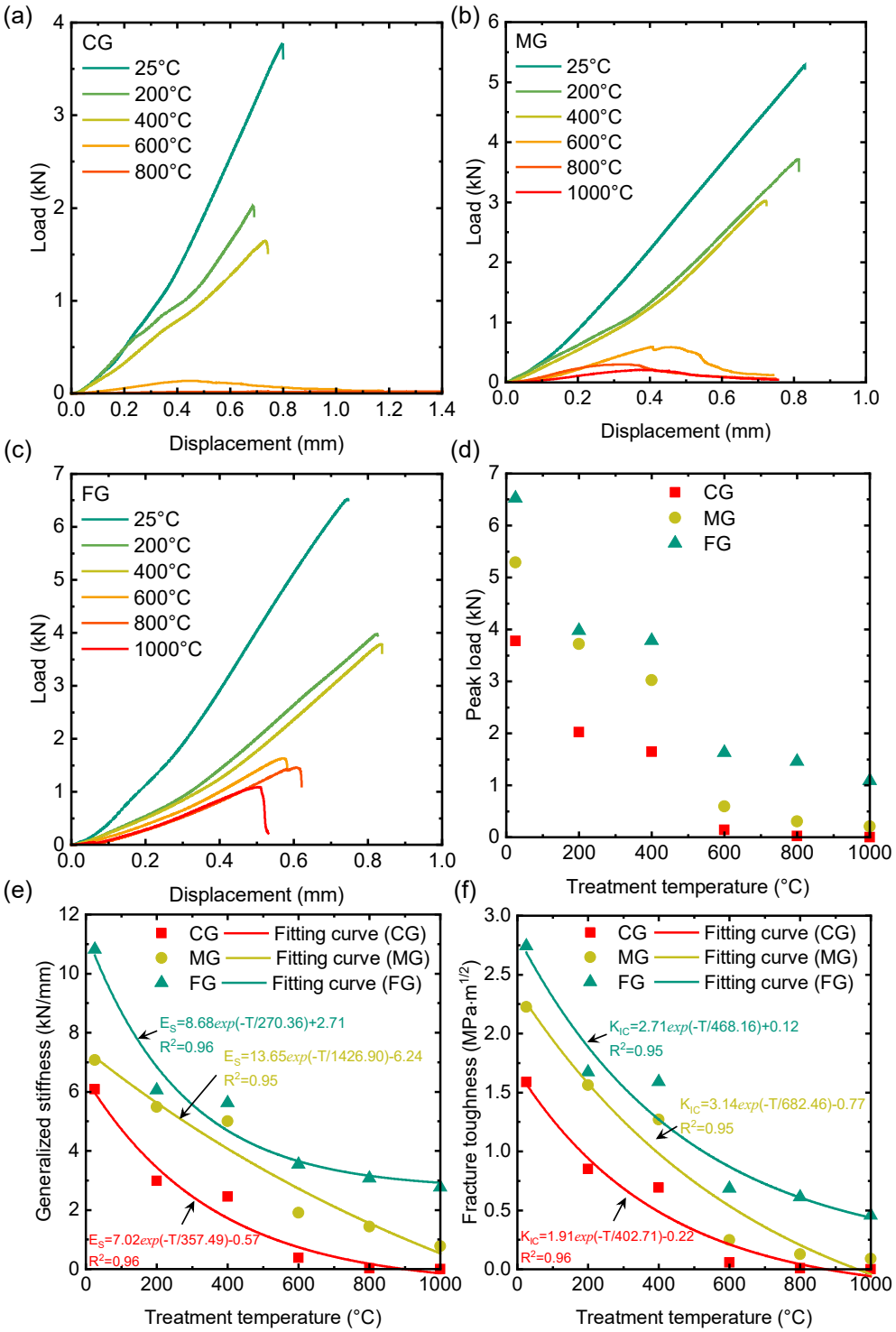

Fig. 10 Mechanical behavior of three types of pre-heated granites. Load-displacement curves of **a** CG samples, **b** MG samples, and **c** FG samples under different temperatures; **d** peak load, **e** generalized stiffness, and **f** fracture toughness of samples after high temperature treatment.

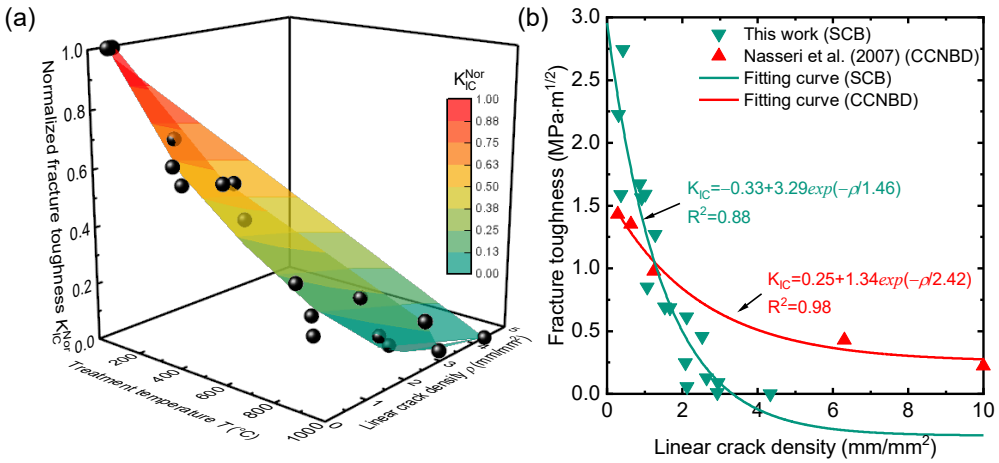

Fig. 11 The relationship between crack density and rock fracture toughness under different temperatures. **a** dependence of normalized fracture toughness of the granite samples on treatment temperature and linear crack density; **b** evolution of the fracture toughness with linear crack density.

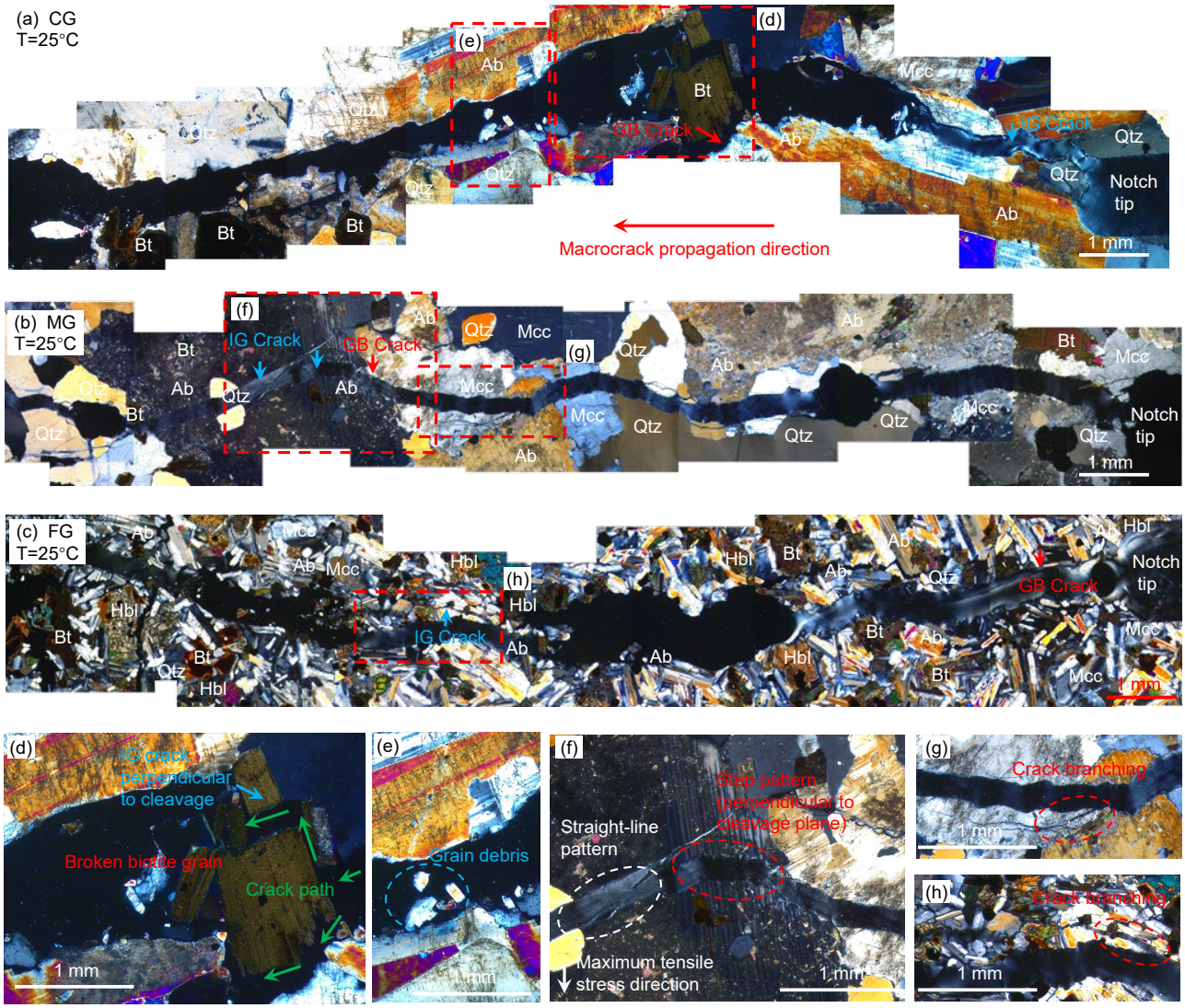

Fig. 12 Fracture path analysis for the CG, MG and FG samples at room temperature. Fracture path of **a** CG sample, **b** MG sample and **c** FG sample under mode I loading; **d** crack path through a biotite grain; **e** grain debris in CG sample; **f** fracture changes from step pattern to straight-line pattern due to mineralogical composition; **g** crack branching in MG sample between microcline and albite; **h** crack branching in FG sample inside albite. Qtz: quartz, Mcc: microcline, Hbl: hornblende, Bt: biotite, Ab: albite.

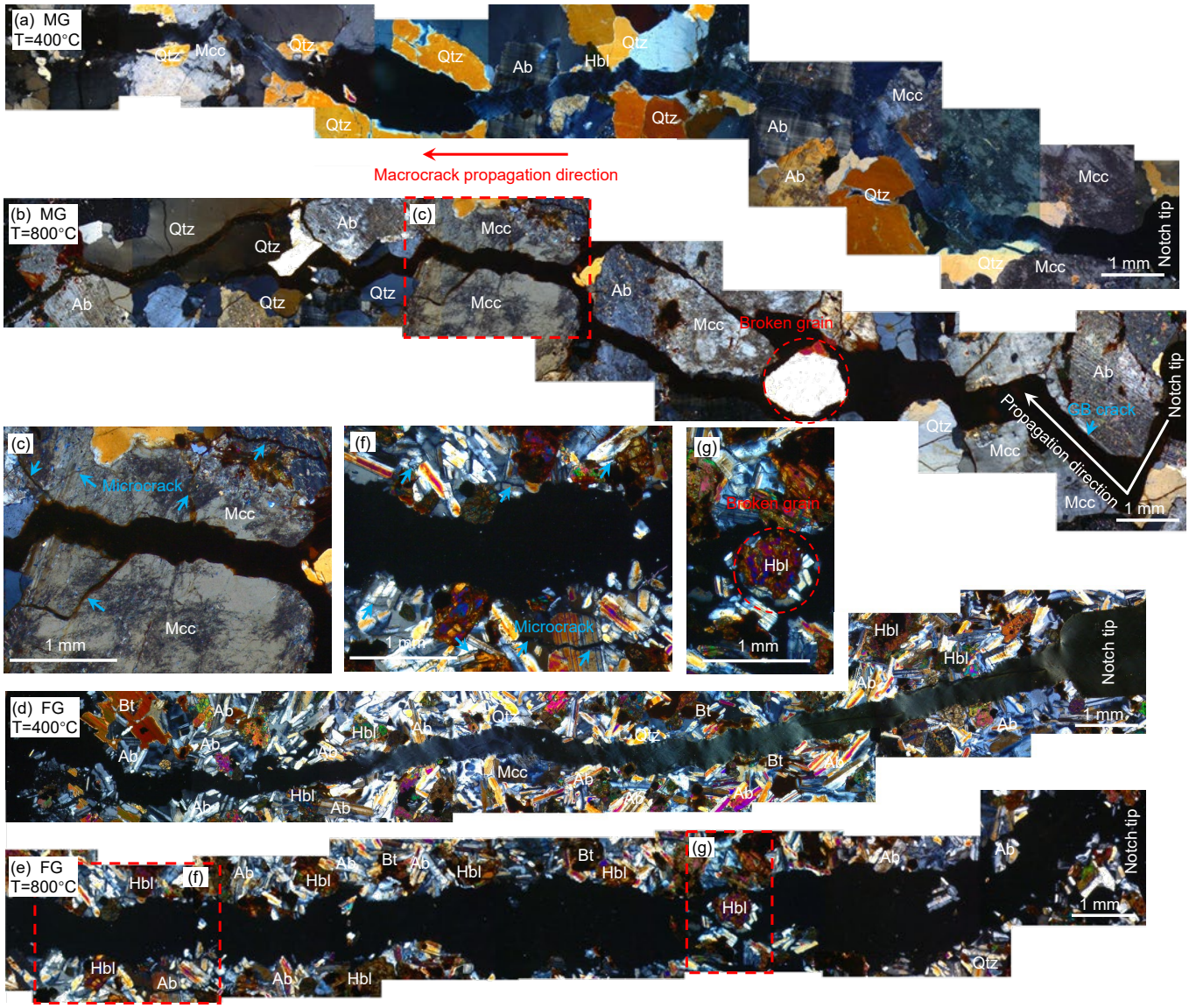

Fig. 13 Fracture path analysis for the MG and FG samples after high temperature treatment. Fracture path of MG sample at **a** 400 °C and **b** 800 °C; **c** the fracture splits the microcline grain into two unequal parts, and there are many thermally induced microcracks distributed around the main macroscopic fracture; fracture path of FG sample at **d** 400 °C and **e** 800 °C; **f** grain missing; **g** a broken hornblende grain in FG sample. Qtz: quartz, Mcc: microcline, Hbl: hornblende, Bt: biotite, Ab: albite.

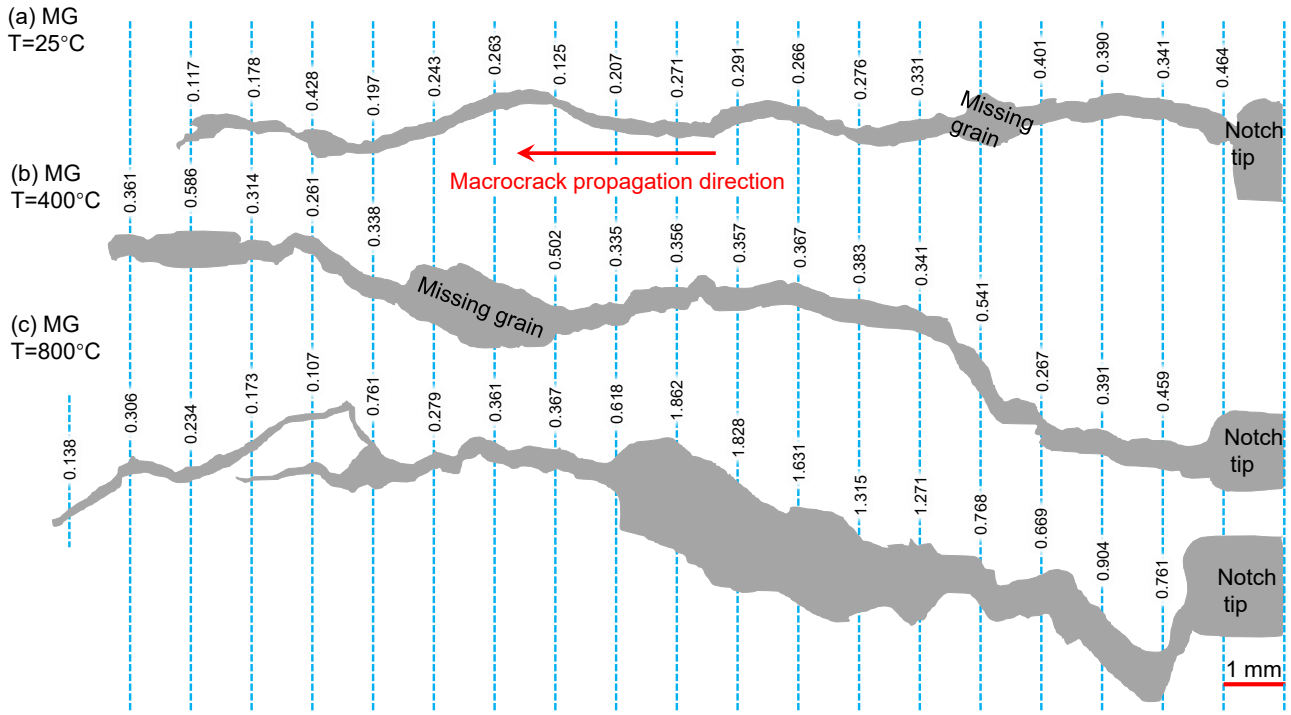

Fig. 14 Fracture path width of MG samples at **a** 25 °C, **b** 400 °C and **c** 800 °C. The value marked in the figures is the fracture path width of the current section with mm unit. When mineral loss occurs, the section is invalid. It is worth noting that the fracture width in pre-heated SCB samples was directly measured from the middle sections, as depicted in Fig. 5.

Table 1 Mineralogical composition of the three rock types at room temperature

Rock type	Quartz (%)	Feldspar (%)		Biotite (%)	Hornblende (%)	Chlorite (%)
		Albite	Microcline			
CG	20.1	36.1	29.8	5.4	4.8	3.8
MG	9.6	30.8	52.9	5.2	0	1.5
FG	3.9	83.4	3.3	7.9	1.5	0

Table 2 The linear thermal crack density of three types of rocks after treatment at different temperatures

Rock type	Linear crack density (mm/mm^2)					
	25 °C	200 °C	400 °C	600 °C	800 °C	1000 °C
CG	0.37	1.07	1.53	2.13	2.93	4.34
MG	0.31	0.92	1.28	2.08	2.65	2.95
FG	0.42	0.87	1.02	1.67	2.12	2.53

Table 3 The tortuosity of MG samples at different temperatures

Temperature (°C)	Nominal length (mm)	Actual length (mm)	Tortuosity	Average width (mm)
25	17.130	17.808	0.925	0.282
400	17.839	19.329	0.852	0.385
800	18.431	21.782	0.716	0.755